Chapter 3

Micromechanics of Piezoelectric Inclusion and Inhomogeneities

3.1. Introduction

In past decades, a number of problems in physics and mechanics of solids have been studied involving the fields generated due to disturbances of a region whose shape and material properties are different from the otherwise uniform surrounding. Eshelby [23,103] provided solution for the stress and strain fields in elastic solids generated due to the presence of an ellipsoidal inclusion or inhomogeneity. These solutions are termed as Eshelby's solution and widely recognized for their elegance and wide-ranging applicability. The methods and results obtained from the analysis serve as the cornerstone of many contemporary micromechanics studies involving defects, fracture, and the behaviour of heterogeneous media at various geometric aspect ratios. Eshelby's solution provides many useful results including the constraint tensors representing transformed fields that arise out of constraint from the surrounding matrix and the equivalent inclusion approach for calculating effective properties of composites. The closed-form expressions known as Eshelby's tensor are the most widely-used result of Eshelby's analyses. These expressions represent a mathematical formulation to model the fields arising due to presence of inhomogeneity as a function of the elastic moduli of the matrix and the shape of the inclusion.

With these tensors in hand, solutions to many complex problems involving inclusions and inhomogeneities are reduced only to algebraic tensor manipulations. In the original work of Eshelby, these tensors were obtained only for inclusions in isotropic solids; it laid the groundwork for the study of inclusions and inhomogeneities in

anisotropic solids, later. Subsequently, the study was extended by researchers [104–110] that provided valuable results regarding inclusions and inhomogeneities in anisotropic solids. For anisotropic solids, no closed form expressions were obtained, hence the Eshelby tensor had to be computed by numerical integration [111]. The *6mm* crystal symmetry also known as transversely isotropic, is of fundamental importance to study piezoelectric inclusion problems because the most important class of piezoelectric materials are poled ceramics exhibiting transverse isotropy with the principal axis aligned along the poling direction. The closed form expressions for Eshelby's tensor are derived for transversely isotropic solids [36,112].

The problem of piezoelectric inclusion and inhomogeneity have been studied by numerous researchers [22,26,113–115], albeit the expressions for the four constraint tensor (piezoelectric analogue of Eshelby's tensor) were not in closed form. Dunn *et. al.* [116] derived expressions for these constraint tensors in the form of surface integrals over a unit sphere which then have been calculated numerically using Gaussian quadrature. Following the work of Withers [36] involving derivation of constraint tensors due to presence of an ellipsoidal inclusion in a transversely isotropic elastic medium, Pan *et. al.* [117] obtained the piezoelectric constraint tensors or Eshelby tensors for a spheroidal inclusion. These tensors were obtained by deriving explicit expressions of Green's functions for a spheroidal inclusion embedded in a transversely isotropic piezoelectric materials problem. Mikata [34,118] obtained explicit expressions for piezoelectric Eshelby tensors for a spheroidal inclusion, but using a different approach. They obtained these tensors by the transformation of the area element representing the piezoelectric Eshelby tensor into integrals for a general ellipsoid inclusion in a transversely isotropic solid.

In this chapter, Section 2 describes an introduction to basic equations of linear piezoelectricity followed by a derivation of inclusion and inhomogeneity problem in a piezoelectric solid. The explicit expressions for the electroelastic Green's functions describing coupled fields and electroelastic Eshelby tensors are discussed in Section 3. In Section 4, an analytical solution is derived to evaluate the effective electroelastic coefficients of a piezoelectric composite with prescribed boundary conditions of traction-electric displacement and elastic displacement-electric field. The explicit closed-form expressions for piezoelectric Eshelby tensors are derived for spheroidal inclusions in transversely isotropic media. A general solution for evaluating piezoelectric Eshelby tensors can be trivially simplified to obtain a solution for many other possible inclusion shapes, e.g., disk-shaped, spherical, and needle-shaped inclusions etc. Up to this point, our approach proceeds in a direction parallel to Eshelby's derivation of the elastic constraint tensors, but there is a departure from Eshelby's approach for the analyses involving electroelastic constraint tensors in an anisotropic media. The novelty of the present approach lies in the use of transformation of variables to yield expressions in the form of surface integrals summed over a unit sphere. The intent of the present work is not to study any one particular aspect of piezoelectric inclusion and inhomogeneities problem; rather the effort is made to make use of these piezoelectric constraint tensors to study the effects of inclusion shape and aspect ratio on the overall properties of piezoelectric composites.

3.2 Governing Equations of Piezoelectricity

A fixed rectangular cartesian coordinate system is considered to describe the local fields at any arbitrary point whose position vector is given by $\boldsymbol{x}$ or x_j $(j = 1,2,3)$. For the analysis, a material that exhibits linear and static coupled-field phenomena has been

considered. It can mathematically be described by three sets of equations, i.e., constitutive, divergence and gradient. Though the inclusion and inhomogeneity problem in a piezoelectric media is explicitly considered at the beginning, in later parts, more emphasis has been laid to the development of a micromechanics model that is valid for a more general coupled-field problem where the basic equations have the same structure. In full index form, the field equations, i.e., constitutive, divergence and gradients are described as:

Constitutive equations:

$$\sigma_{ij} = C_{ijmn}\varepsilon_{mn} - e_{nij}E_n \tag{3.1}$$

$$D_i = e_{imn}\varepsilon_{mn} + \kappa_{in}E_n \tag{3.2}$$

where C_{ijmn}, e_{nij}, κ_{in} are the elastic constants measured at a constant electric field, the piezoelectric coefficients measured at a constant strain or electric field, dielectric constants measured at a constant strain, respectively. The elastic strain, ε_{mn} and electric field, E_n are related to stress, σ_{ij} and electric displacement, D_i as shown in Eqns. (3.1) and (3.2).

Divergence equations:

$$\sigma_{ij,j} = 0 \tag{3.3}$$

$$D_{i,i} = 0 \tag{3.4}$$

where σ_{ij} and D_i are the stress and the electric displacement, respectively.

Gradient equations:

$$\varepsilon_{ij} = \frac{1}{2}(u_{i,j} + u_{j,i}) \tag{3.5}$$

$$E_i = -\phi_{,i} \tag{3.6}$$

In the above equations, u_i and ϕ are the elastic displacement and the electric potential, respectively.

While deriving the solution for piezoelectric boundary value problems, it is convenient to treat the elastic and electric variables on equal parameters. To further the analysis, the notation introduced by Barnett *et. al.* [119] is employed. This notation is almost similar to the conventional indicial notation, but with the exception of both the lowercase and uppercase subscripts being used as indices. Lowercase subscripts are set to take the range of *1, 2, 3,* while uppercase subscripts are set to take the range *1, 2, 3, 4;* in addition, repeated uppercase subscripts are summed over *1→4*. Following above notation, the elastic strain and electric field are expressed as:

$$Z_{Mn} = \begin{cases} \varepsilon_{mn} & M = 1,2,3 \\ -E_n & M = 4 \end{cases} \tag{3.7}$$

where Z_{Mn} is derivable from the generalized potential represented by U_M and described as:

$$U_M = \begin{cases} u_m & M = 1,2,3 \\ \phi & M = 4 \end{cases} \tag{3.8}$$

Similarly, the stress and electric displacement can be conveniently represented as:

$$\Sigma_{iJ} = \begin{cases} \sigma_{ij} & J = 1,2,3 \\ D_i & J = 4 \end{cases} \tag{3.9}$$

The electroelastic moduli, L_{iJMn} can then be represented in combined form as:

$$L_{iJMn} = \begin{cases} C_{ijmn} & J, M = 1,2,3 \\ e_{nij} & J = 1,2,3;\ M = 4 \\ e_{imn} & J = 4; M = 1,2,3 \\ -\kappa_{in} & J, M = 4 \end{cases} \tag{3.10}$$

The inverse of L_{iJMn} is defined as $\bar{L}_{AbiJ}$. The symmetry properties of L_{iJMn} remain conserved and are easily derivable from those of C_{ijmn}, e_{nij}, and κ_{in}. With this shorthand notation, Eqns. (3.1) and (3.2) can be unified into a single equation:

$$\Sigma_{iJ} = L_{iJMn} Z_{Mn} \tag{3.11}$$

or inverting the above equation:

$$Z_{Ab} = \bar{L}_{AbiJ} \Sigma_{iJ} \tag{3.12}$$

Here, it is important to note that Z_{Mn}, U_M, Σ_{iJ}, L_{iJMn}, and $\bar{L}_{AbiJ}$ are not tensors. Thus, while considering corresponding equations is an alternate coordinate system, each individual tensor must be transformed first with the laws of tensor transformation. Later, the resulting tensors can be reunified to the form of Eqns. (3.7) - (3.10).

3.3 Piezoelectric Inclusion and Inhomogeneities

In this section, the coupled electroelastic fields due to an inclusion or inhomogeneity present in an infinite matrix are derived in a manner analogous to the classical work of Eshelby's for studying elastic fields [22]. The Deeg's approach to study inclusion problems in a piezoelectric media [22], is used to obtain four constraint tensors analogous to Eshelby's tensor for the elasticity problem. The use of these constraint tensors is pivotal to model the coupled field phenomena, and these constraint tensors are of primary importance to study numerous inclusion and inhomogeneity problems in piezoelectric solids.

First, consider an infinite piezoelectric solid containing an inclusion of ellipsoidal shape, and the geometry of inclusion is defined by

$$(x_1/a_1)^2 + (x_2/a_2)^2 + (x_3/a_3)^2 = 1 \tag{3.13}$$

where a_1, a_2, and a_3 are the lengths of the semi-axes of the ellipsoidal inclusion. The domain of the inclusion is represented by Ω, its surface by $|\Omega|$; and the entire domain by *D*. The electroelastic moduli of inclusion is same as of the matrix, L_{iJMn}. The inclusion is allowed to undergo a uniform stress-free strain, ε^*_{mn}, and electric displacement-free electric field, E^*_n, represented by a combined notation, Z^*_{Mn}. These uniform stress-free strains and electric displacement-free electric fields do occur due to various physical phenomena which includes phase transformation, thermal expansion coefficient mismatch, pyroelectric coefficient mismatch, etc. Now, to calculate the stress, strain, electric displacement, and electric field developed due to such misfits; an analytical model based on the imaginary cutting, straining, and welding operations is utilized [23].

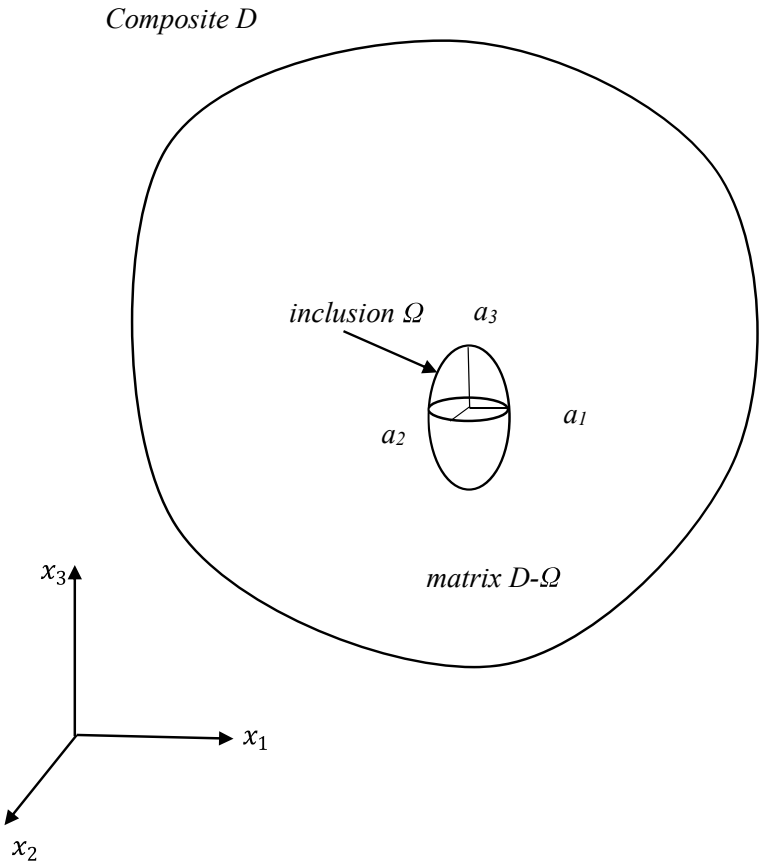

Figure 3.1(a) Schematic of an ellipsoidal inclusion in a matrix medium.

In the beginning, the individual state of inclusion and matrix are free of any stress and electric displacement, i.e., $\Sigma_{iJ}^{\Omega} = \Sigma_{iJ}^{m} = 0$; the superscripts Ω and m denote the domains of the inclusion and matrix, respectively. The inclusion is then removed from the matrix around the surface $|\Omega|$ by cutting operations. The removed portion is then allowed to undergo the uniform unconstrained transformations termed as eigen strain and electric field, Z_{Mn}^{*}. In both the inclusion and matrix, the stress and electric displacement remains zero, i.e., $\Sigma_{iJ}^{\Omega} = \Sigma_{iJ}^{m} = 0$. But now, the inclusion will not fit into the same cavity either mechanically or electrically on its own. An external force or field must be applied to the inclusion to make it fit to the same cavity. The inclusion is then deformed back to its original shape or mechanical and electrical state by applying tractions and electric displacement normal to the surface of inclusion around $|\Omega|$. The external agent required to deform the inclusion to its original shape can be mathematically described as:

$$T_J = -\Sigma_{iJ}^{*} n_i \tag{3.14}$$

In Eqn. (3.14), T_J can be considered to be the layers of body force and surface charge and Σ_{iJ}^{*} be the external stress and electric displacement that is required to cause eigen fields, Z_{Mn}^{*}. Mathematically this relation can be expressed as, $\Sigma_{iJ}^{\Omega} = L_{iJMn} Z_{Mn}^{*}$. Now, the inclusion is put back into the cavity and rewelded. The layer considered to be of body force and surface charge is then nullified by applying a traction and normal electric displacement or $-T_J$ over $|\Omega|$. A resulting stress and electric displacement field would now exist in the inclusion and matrix due to the presence of $T_J = -\Sigma_{iJ}^{*} n_i$ over domain $|\Omega|$. To explain these fields, an analytic expression is desired.

Following the transformation of the inclusion, the elastic displacement and electric potential, U_M, can be expressed in terms of electroelastic Green's functions, denoted by $G_{MJ}(\boldsymbol{x} - \boldsymbol{x}')$ and mathematically derived as [22,27]:

$$U_M(\boldsymbol{x}) = \iint_{|\Omega|} G_{MJ}(\boldsymbol{x}-\boldsymbol{x}')\,\Sigma^*_{ij} n_i dS(\boldsymbol{x}') - \iint_{\Omega}\int G_{MJ}\,(\boldsymbol{x}-\boldsymbol{x}')\Sigma^*_{ij,i} dV(\boldsymbol{x}') \tag{3.15}$$

where n_i is the outward normal to $|\Omega|$. In all the mathematical expressions, bold face characters denote vectors. In Eqn. (3.15), the Green's functions, $G_{MJ}(\boldsymbol{x}-\boldsymbol{x}')$ have physical interpretations as the field effects generated at a given point due to presence of unit point charge or stress at a reference point within the inclusion [22], and can be expressed as:

$$G_{MJ}(\boldsymbol{x}-\boldsymbol{x}') = \frac{1}{8\pi^2|\boldsymbol{x}-\boldsymbol{x}'|}\int_{|z|=1} K^{-1}_{MR}\delta(\boldsymbol{z}.\boldsymbol{t})\,dS(\boldsymbol{z}) \tag{3.16}$$

In the above equation, $\delta(\boldsymbol{x})$ denotes the Dirac-delta function, $|z|$ denotes the surface of a unit sphere whose centre is at origin, i.e., z=0 and K^{-1}_{MR} is the inverse of the following expressions:

$$K_{JR} = z_i z_n L_{iJRn} \tag{3.17}$$

In Eqn. (3.16), $\boldsymbol{t}$ is a unit vector in the direction of $\boldsymbol{x}-\boldsymbol{x}'$, and expressed as: $\boldsymbol{t} = (\boldsymbol{x}-\boldsymbol{x}')/|\boldsymbol{x}-\boldsymbol{x}'|$.

Using Gauss divergence theorem and the mathematical correlation (due to symmetry) $\partial G_{MJ}(\boldsymbol{x}-\boldsymbol{x}')/\partial \boldsymbol{x}'_i = -\partial G_{MJ}(\boldsymbol{x}-\boldsymbol{x}')/\partial \boldsymbol{x}_i$, Eqn. (3.15) can be expressed in form of volume integral over the inclusion with $G_{MJ,in}(\boldsymbol{x}-\boldsymbol{x}')\Sigma^*_{ij}$ in the integrand. It is then further simplified considering the fact that $\Sigma^*_{ij} = L_{iJMn}Z^*_{Mn}$ is uniform inside Ω, $U_{M,n}(\boldsymbol{x})$ can now be expressed as:

$$U_{M,n}(\boldsymbol{x}) = -L_{iJAb}Z^*_{Ab}\iint_{\Omega}\int G_{MJ,in}\,(\boldsymbol{x}-\boldsymbol{x}')\,dV(\boldsymbol{x}') \tag{3.18}$$

Following the works of Deeg, Asaro *et. al.* and Willis [22,24,120], the Green's function $G_{MJ,in}(\boldsymbol{x}-\boldsymbol{x}')$ can be written in terms of Dirac delta function and K^{-1}_{MR} as:

$$G_{MJ,in}(\boldsymbol{x}-\boldsymbol{x}')=\frac{1}{8\pi^2}\frac{\partial^2}{\partial x_k \partial x_k}\int_{|z|=1} z_i z_n K_{MJ}^{-1}(\boldsymbol{z})\delta[\boldsymbol{z}.(\boldsymbol{x}-\boldsymbol{x}')]dS(\boldsymbol{z}) \tag{3.19a}$$

The integration shown in above equation is surface integral over the unit sphere $|z|=1$. To determine $U_{M,n}(\boldsymbol{x})$ for any point inside the ellipsoidal inclusion, the point of observation $\boldsymbol{x}$ is taken inside $\boldsymbol{\Omega}$ followed by parameterization of the ellipsoid $\boldsymbol{\Omega}$ over a unit sphere. By making use of properties of Dirac delta function, an equilibrium condition is derived for the coupled electroelastic Green's function and it is written as follows:

$$L_{iJMn}G_{MA,in}(\boldsymbol{x}-\boldsymbol{x}')+\delta_{JA}\delta(\boldsymbol{x}-\boldsymbol{x}')=0 \tag{3.19b}$$

Few mathematical manipulations over Eqn. (3.19a) by using the equilibrium condition of Eqn. (1.19b); followed by partial derivative with respect x_k leads to the following expression:

$$U_{M,n}(\boldsymbol{x})=\frac{a_1 a_2 a_3}{4\pi}L_{iJAb}Z_{Ab}^{*}\int_{|z|=1}\frac{1}{\zeta^3}z_i z_n K_{MJ}^{-1}(\boldsymbol{z})d\Omega(\boldsymbol{z}) \tag{3.20}$$

where,
$$\zeta=[a_1^2 z_1^2+a_2^2 z_2^2+a_3^2 z_3^2]^{\frac{1}{2}} \tag{3.21}$$

Because of linearity, the induced strain and electric field due to the uniform eigenfield can be expressed as linear functions of Z_{Mn}^{*}, and expressed as:

$$Z_{Mn}(\boldsymbol{x})=S_{MnAb}Z_{Ab}^{*} \tag{3.22}$$

here $\boldsymbol{x}$ represents a reference point in the interior of the ellipsoid inclusion again. Using Eqns. (3.5), (3.6), (3.7), and (3.20), the set of electroelastic Eshelby tensors, S_{MnAb} can be expressed as:

$$S_{MnAb} = \begin{cases} \frac{a_1 a_2 a_3}{8\pi} L_{iJAb} \int_{|z|=1} \frac{1}{\zeta^3} \left[G_{mJin}(\boldsymbol{z}) + G_{nJim}(\boldsymbol{z}) \right] dS(\boldsymbol{z}), & M = 1,2,3 \\ \frac{a_1 a_2 a_3}{4\pi} L_{iJAb} \int_{|z|=1} \frac{1}{\zeta^3} G_{4Jin}(\boldsymbol{z}) dS(\boldsymbol{z}), & M = 4, \end{cases} \quad (3.23)$$

where,

$$G_{MJin}(\boldsymbol{z}) = z_i z_n K_{MJ}^{-1}(\boldsymbol{z}). \quad (3.24)$$

Eqn. (3.23) shows the integral to be applied over surface of a contour $|z| = 1$. For evaluating the integrals in Eqn. (3.23), a transformation of the surface element $dS(\boldsymbol{z})$ to a new surface element $dS(\boldsymbol{\xi})$ is carried out as:

$$\xi_1 = a_1 z_1/\zeta, \quad \xi_2 = a_2 z_2/\zeta, \quad \xi_3 = a_3 z_3/\zeta \quad (3.25)$$

where ζ is defined by Eqn. (3.21). The transformed surface element, $dS(\boldsymbol{\xi})$ is related to the initial surface element, $dS(\boldsymbol{z})$ by:

$$dS(\boldsymbol{\xi}) = a_1 a_2 a_3/\zeta^3 \, dS(\boldsymbol{z}) \quad (3.26)$$

With the transformations performed in accordance to Eqn. (3.25) and (3.26), Eqn. (3.23) can now be expressed as:

$$S_{MnAb} = \begin{cases} \frac{1}{8\pi} L_{iJAb} \int_{-1}^{1} \int_{0}^{2\pi} \left[G_{mJin}(\boldsymbol{z}) + G_{nJim}(\boldsymbol{z}) \right] dS(\boldsymbol{z}) \, d\theta d\xi_3, & M = 1,2,3, \\ \frac{1}{4\pi} L_{iJAb} \int_{-1}^{1} \int_{0}^{2\pi} \left[G_{mJin}(\boldsymbol{z}) + G_{nJim}(\boldsymbol{z}) \right] dS(\boldsymbol{z}) \, d\theta d\xi_3 & M = 4. \end{cases} \quad (3.27)$$

It should also be noted that, the functions $G_{MJin}(\boldsymbol{z})$ in Eqn. (3.27) are homogeneous functions of degree zero, hence the transformations shown in Eqn. (3.25) reduced to:

$$z_1 = \xi_1/a_1, \quad z_2 = \xi_2/a_2, \quad z_3 = \xi_3/a_3, \quad (3.28)$$

further, ξ_1 and ξ_2 can easily be manipulated in terms of ξ_3, and the spherical polar angle, θ, as

$$\xi_1 = (1-\xi_3^2)^{\frac{1}{2}} cos\theta, \quad \xi_2 = (1-\xi_3^2)^{\frac{1}{2}} sin\theta, \quad \xi_3 = \xi_3. \tag{3.29}$$

It is seen from the Eqn. (3.27) that the resulting electroelastic Eshelby tensors are functions of the shape of inclusion and the properties of the surrounding matrix. Also, Eqn. (3.22) suggests the induced strain and electric field is a linear function of uniform prescribed eigenstrains Z^*_{Mn}. It may be concluded from the Eqns. (3.22) and (3.27) that the strain, ε_{mn}, and the electric field, E_n, inside the inclusion is uniform for the coupled problem, in line with the uncoupled elastic and electric problems [23,30].

The set of electroelastic Eshelby tensors as shown in Eqn. (3.27) can be expressed explicitly in terms of the electroelastic moduli or constituents' properties as:

$$S_{mnab} = \frac{1}{8\pi}\left\{ C_{ijab} \int_{-1}^{1}\int_{0}^{2\pi} \left[G_{mjin}(\boldsymbol{z}) + G_{njim}(\boldsymbol{z})\right] d\theta d\xi_3 - e_{iab} \int_{-1}^{1}\int_{0}^{2\pi} \left[G_{m4in}(\boldsymbol{z}) + G_{n4im}(\boldsymbol{z})\right] d\theta d\xi_3 \right\}, \tag{3.30}$$

$$S_{mn4b} = \frac{1}{8\pi}\left\{ e_{bij} \int_{-1}^{1}\int_{0}^{2\pi} \left[G_{mjin}(\boldsymbol{z}) + G_{njim}(\boldsymbol{z})\right] d\theta d\xi_3 + \kappa_{ib} \int_{-1}^{1}\int_{0}^{2\pi} \left[G_{m4in}(\boldsymbol{z}) + G_{n4im}(\boldsymbol{z})\right] d\theta d\xi_3 \right\}, \tag{3.31}$$

$$S_{4nab} = \frac{1}{4\pi}\left\{ C_{ijab} \int_{-1}^{1}\int_{0}^{2\pi} G_{4jin}(\boldsymbol{z})\, d\theta d\xi_3 - e_{iab} \int_{-1}^{1}\int_{0}^{2\pi} G_{44in}(\boldsymbol{z})\, d\theta d\xi_3 \right\}, \tag{3.32}$$

$$S_{4nab} = \frac{1}{4\pi}\left\{ e_{bij} \int_{-1}^{1}\int_{0}^{2\pi} G_{4jin}(\boldsymbol{z})\, d\theta d\xi_3 + \kappa_{ib} \int_{-1}^{1}\int_{0}^{2\pi} G_{44in}(\boldsymbol{z})\, d\theta d\xi_3 \right\}, \tag{3.33}$$

The electroelastic constraint tensors S_{MnAb} as defined in Eqn. (3.27) and (3.30) - (3.33) will represent the stress and electric displacement in the transformed inclusion due to the constraint of the surrounding medium. These electroelastic constraint tensors are seen to be functions of the material properties of matrix and the shape of the inclusion. When piezoelectric coupling is ignored, Eqn. (3.31) and (3.32) vanish and (3.30) and (3.33) reduce to the well-known Eshelby tensors in elasticity, which suggests that these tensors are piezoelectric analogue to the Eshelby tensors in elasticity.

3.3.1 Evaluation of Electroelastic Green's Functions

To be specific, the solution to Eqn. (3.18) will provide the elastic displacement and electric potential at some observing point $\boldsymbol{x}'$, when a unit point force or a unit point charge is applied to the reference point $\boldsymbol{x}$. Due to the presence of electroelastic coupling, the electric charge will induce an electric field as well as an elastic displacement. Similarly, the stress will induce an elastic displacement, and also an electric field. The electroelastic Green's functions are represented by $G_{MJ}(\boldsymbol{x}-\boldsymbol{x}')$, and have these following physical interpretations:

$G_{mj}(\boldsymbol{x}-\boldsymbol{x}')=$ the elastic displacement at $\boldsymbol{x}$ in the x_m-direction due to a unit point force at $\boldsymbol{x}'$ in the x_j-direction;

$G_{m4}(\boldsymbol{x}-\boldsymbol{x}')=$ the elastic displacement at $\boldsymbol{x}$ in the x_m-direction due to a unit point charge at $\boldsymbol{x}'$;

$G_{4j}(\boldsymbol{x}-\boldsymbol{x}')=$ the electric potential at $\boldsymbol{x}$ in the x_m-direction due to a unit point force at $\boldsymbol{x}'$ in the x_j-direction;

$G_{44}(\boldsymbol{x}-\boldsymbol{x}')=$ the electric potential at $\boldsymbol{x}$ due to a unit point charge at $\boldsymbol{x}'$.

For an infinite heterogeneous piezoelectric solid, these infinite body Green's functions, denoted by $G_{MR}(\boldsymbol{x}, \boldsymbol{x}')$ directly depend on the relative position of the point source at, $\boldsymbol{x}'$, with reference to an observer at, $\boldsymbol{x}$. It can be represented as $G_{MR}(\boldsymbol{x} - \boldsymbol{x}')$ also, or, $G_{MR}(\boldsymbol{x}, \boldsymbol{x}') = G_{MR}(\boldsymbol{x} - \boldsymbol{x}')$. These electroelastic Green's functions $G_{MR}(\boldsymbol{x} - \boldsymbol{x}')$ must satisfy the following differential equations:

$$E_{iJMn} G_{MR,in}(\boldsymbol{x} - \boldsymbol{x}') + \delta_{JR}\delta(\boldsymbol{x} - \boldsymbol{x}') = 0 \tag{3.34}$$

In the above equation, $\delta(\boldsymbol{x} - \boldsymbol{x}')$ represents the three-dimensional Dirac delta function and δ_{JR} is the generalized Kronecker delta. The essential boundary conditions on $G_{MR}(\boldsymbol{x} - \boldsymbol{x}')$ are that the first spatial partial derivative and the value of the function itself must vanish as $|\boldsymbol{x} - \boldsymbol{x}'| \to \infty$, and are seen to satisfy the identity given by Eqn. (3.34).

To simplify the analysis, let us consider transversely isotropic symmetry of the piezoelectric material specifically. Adopting Voigt two-index notation [5], the constitutive relation given by Eqn. (3.11) reduces to the following forms:

$$\begin{aligned}
\sigma_{11} &= C_{11}\varepsilon_{11} + C_{12}\varepsilon_{22} + C_{13}\varepsilon_{33} - e_{31}E_3 \\
\sigma_{22} &= C_{12}\varepsilon_{11} + C_{11}\varepsilon_{22} + C_{13}\varepsilon_{33} - e_{31}E_3 \\
\sigma_{33} &= C_{13}\varepsilon_{11} + C_{13}\varepsilon_{22} + C_{33}\varepsilon_{33} - e_{33}E_3 \\
\sigma_{23} &= C_{44}\varepsilon_{23} - e_{15}E_1 \\
\sigma_{13} &= C_{44}\varepsilon_{13} - e_{15}E_2 \\
\sigma_{12} &= C_{66}\varepsilon_{12} \\
D_1 &= e_{15}\varepsilon_{13} + \kappa_{11}E_1 \\
D_2 &= e_{15}\varepsilon_{23} + \kappa_{11}E_2 \\
D_3 &= e_{31}(\varepsilon_{11} + \varepsilon_{22}) + e_{33}\varepsilon_{33} + \kappa_{33}E_3
\end{aligned} \tag{3.35}$$

Following the transversely isotropic symmetry conditions, the matrix $K_{MR}(\boldsymbol{z})$ as shown in Eqn. (3.16) can be expressed as:

$$K_{MJ}(\boldsymbol{z}) = \begin{bmatrix} \varpi_1 z_1^2 + \varpi_4 z_2^2 + \varpi_5 z_3^2 & (\varpi_1 - \varpi_4) z_1 z_2 & \varpi_3 z_1 z_3 & \varpi_6 z_1 z_3 \\ (\varpi_1 - \varpi_4) z_1 z_2 & \varpi_4 z_1^2 + \varpi_1 z_2^2 + \varpi_5 z_3^2 & \varpi_3 z_2 z_3 & \varpi_6 z_2 z_3 \\ \varpi_3 z_1 z_3 & \varpi_3 z_2 z_3 & \varpi_5 (z_1^2 + z_2^2) + \varpi_2 z_3^2 & \varpi_7 (z_1^2 + z_2^2) + \varpi_8 z_3^2 \\ \varpi_6 z_1 z_3 & \varpi_6 z_2 z_3 & \varpi_7 (z_1^2 + z_2^2) + \varpi_8 z_3^2 & \varpi_9 (z_1^2 + z_2^2) + \varpi_0 z_3^2 \end{bmatrix} \tag{3.36}$$

where,

$$\begin{aligned} &\varpi_1 = C_{11} && \varpi_2 = C_{33} && \varpi_3 = C_{13} + C_{44} \\ &\varpi_4 = \tfrac{1}{2}(C_{11} - C_{12}) && \varpi_5 = C_{44} && \varpi_6 = e_{31} + e_{15} \\ &\varpi_7 = e_{15} && \varpi_8 = e_{33} && \varpi_9 = -\kappa_{11} \\ &\varpi_0 = -\kappa_{33} \end{aligned} \tag{3.37}$$

The terms $\varpi_1 - \varpi_5$ in the Eqn. (3.37) represent the elastic effects and coincide with those discussed by the author [105], the additional terms $\varpi_6 - \varpi_8$ and $\varpi_9 - \varpi_0$ represent the piezoelectric and dielectric effects, respectively. The inverse of the matrix, $K_{MJ}(\boldsymbol{z})$ shown in Eqn. (3.36) can be expressed as:

$$K_{MJ}^{-1}(\boldsymbol{z}) = \frac{1}{D}\begin{bmatrix} r_{11} & r_{12} & r_{13} & r_{14} \\ r_{21} & r_{22} & r_{23} & r_{24} \\ r_{31} & r_{32} & r_{33} & r_{34} \\ r_{41} & r_{42} & r_{43} & r_{44} \end{bmatrix} \tag{3.38}$$

where,

$$\begin{aligned} r_{11} &= (\eta_{111} z_1^2 + \eta_{112} z_2^2)\gamma^2 + (\eta_{113} z_1^2 + \eta_{114} z_2^2) z_3^2 \gamma \\ &\quad + (\eta_{115} z_1^2 + \eta_{116} z_2^2) z_3^4 + r_{117} z_3^6 \\ r_{12} &= z_1 z_2 (\eta_{121} \gamma^2 + \eta_{122} \gamma z_3^2 + \eta_{123} z_3^4) \end{aligned}$$

$$r_{13} = z_1 z_3 P(\eta_{131}\gamma + \eta_{132} z_3^2)$$

$$r_{14} = z_1 z_3 P(\eta_{141}\gamma + \eta_{142} z_3^2)$$

$$r_{21} = b_{12}$$

$$r_{22} = (\eta_{221} z_1^2 + \eta_{222} z_2^2)\gamma^2 + (\eta_{223} z_1^2 + \eta_{224} z_2^2) x_3^2 \gamma + (\eta_{225} z_1^2 + \eta_{226} z_2^2) z_3^4 + \eta_{227} z_3^6$$

$$r_{23} = z_2 z_3 P(\eta_{231}\gamma + \eta_{232} z_3^2)$$

$$r_{24} = z_2 z_3 P(\eta_{241}\gamma + \eta_{242} z_3^2)$$

$$r_{31} = r_{13}$$

$$r_{32} = r_{23}$$

$$r_{33} = P(\eta_{331}\gamma^2 + \eta_{332}\gamma z_3^2 + \eta_{333} z_3^4)$$

$$r_{34} = P(\eta_{341}\gamma^2 + \eta_{342}\gamma z_3^2 + \eta_{343} z_3^4)$$

$$r_{41} = r_{14}$$

$$r_{42} = r_{24}$$

$$r_{43} = r_{34}$$

$$r_{44} = P(\eta_{441}\gamma^2 + \eta_{442}\gamma z_3^2 + \eta_{443} z_3^4) \quad (3.39)$$

and,

$$D(z_1, z_2, z_3) = -PQ$$

$$P(z_1, z_2, z_3) = (C_{11} - C_{12})\gamma + 2C_{44} z_3^2$$

$$Q(z_1, z_2, z_3) = q_1\gamma^3 + q_2\gamma^2 z_3^2 + q_3\gamma z_3^2 + q_4 z_3^6$$

$$\gamma = z_1^2 + z_2^2 \quad (3.40)$$

The parameters q_i $(i = 1 - 4)$ and η_{ijk} shown in Eqns. (3.39) and (3.40) seem to be functions of constituent's material properties, and are listed in Appendix B. K_{MJ}^{-1} shown in Eqn. (3.16) is a symmetric matrix that leads to the symmetry of the Green's functions and represented as:

$$G_{MJin} = G_{JMin} \tag{3.41}$$

3.3.2 Electroelastic Eshelby Tensors for Spheroidal Inclusion

A spheroid inclusion aligned along the x_3-axis (see Figure 3.2) can be parametrized as follows

$$a_1 = a, \qquad \frac{a_1}{a_2} = 1, \qquad \frac{a_1}{a_3} = \beta \tag{3.42}$$

Substituting Eqn. (3.42) into (3.24), the expression of electroelastic Green's function can also be written as

$$\begin{aligned} \bar{G}_{MJin} &= \int_{|z|=1} G_{MJin}\left(\frac{z_1}{a}, \frac{z_2}{a}, \frac{\beta z_3}{a}\right) dS \\ &= \int_{|z|=1} G_{MJin}(z_1, z_2, \beta z_3) \end{aligned} \tag{3.43}$$

Since, $G_{MJin}(\boldsymbol{x})$ is a homogeneous function of order zero, the integral shown with the second equality is equivalent to the first one. Substituting Eqn. (3.24) into (3.43), the non-zero components of $\bar{G}_{MJin}$ can be expressed as

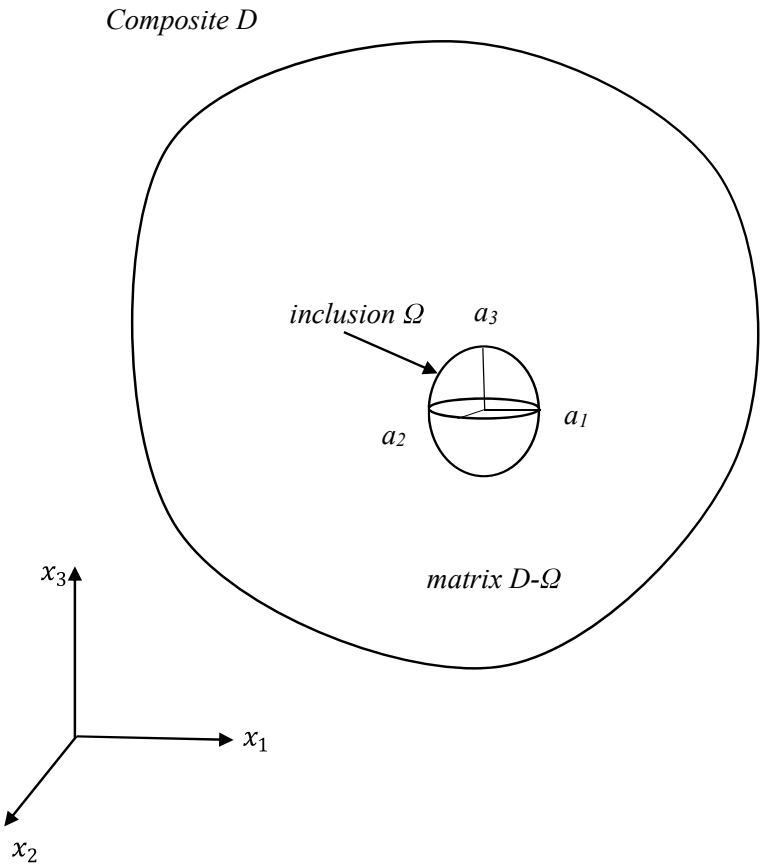

Figure 3.1(b) Schematic of a spheroidal inclusion in a matrix medium.

$$\bar{G}_{MJ11} = \int_{|z|=1} z_1^2 K_{MJ}^{-1}(z_1, z_2, \beta z_3)\, dS$$

$$\bar{G}_{MJ22} = \int_{|z|=1} z_2^2 K_{MJ}^{-1}(z_1, z_2, \beta z_3)\, dS$$

$$\bar{G}_{MJ33} = \int_{|z|=1} \beta^2 z_3^2 K_{MJ}^{-1}(z_1, z_2, \beta z_3)\, dS$$

$$\bar{G}_{1212} = \int_{|z|=1} z_1 z_2 K_{MJ}^{-1}(z_1, z_2, \beta z_3)\, dS$$

$$\bar{G}_{1313} = \int_{|z|=1} \beta z_1 z_3 K_{MJ}^{-1}(z_1, z_2, \beta z_3)\, dS$$

$$\bar{G}_{1314} = \int_{|z|=1} \beta z_1 z_3 K_{MJ}^{-1}(z_1, z_2, \beta z_3)\, dS$$

$$\bar{G}_{2323} = \int_{|z|=1} \beta z_2 z_3 K_{MJ}^{-1}(z_1, z_2, \beta z_3)\, dS$$

$$\bar{G}_{2324} = \int_{|z|=1} \beta z_2 z_3 K_{MJ}^{-1}(z_1, z_2, \beta z_3)\, dS \tag{3.44}$$

To solve the surface integral in above expressions, unit sphere must be first parametrized as follows

$$z_1 = sin\theta cos\varphi, \;\; z_2 = sin\theta sin\varphi, \;\; z_3 = cos\theta, 0 \le \theta \le \pi, \;\; 0 \le \varphi \le 2\pi. \tag{3.45}$$

With above parameters, the area element dS is transformed to

$$dS = sin\theta d\theta d\varphi \tag{3.46}$$

Substituting Eqns. (3.45) and (3.46) into Eqn. (3.44), and integrating the integrand with respect to φ, followed by the replacement of variables θ by t with following parametrization

$$t = cos\theta, \quad dt = -sin\theta d\theta, \quad sin^2\theta = 1 - t^2, \tag{3.47}$$

the electroelastic Green's functions G_{MJin} can be finally derived as

$$\bar{G}_{1111} = \frac{\pi}{2}\int_0^1 \frac{1-t^2}{D}[(3\eta_{111} + \eta_{112})(1-t^2)^3 + \beta^2(3\eta_{113} + \eta_{114})(1-t^2)^2 t^2 + \beta^4(3\eta_{115} + \eta_{116})(1-t^2)t^4 + 4\beta^6\eta_{117}t^6]dt$$

$$\bar{G}_{1122} = \frac{\pi}{2}\int_0^1 \frac{1-t^2}{D}[(3\eta_{221} + \eta_{222})(1-t^2)^3 + \beta^2(3\eta_{223} + \eta_{224})(1-t^2)^2 t^2 + \beta^4(3\eta_{225} + \eta_{226})(1-t^2)t^4 + 4\beta^6\eta_{227}t^6]dt$$

$$\bar{G}_{1133} = -2\pi\int_0^1 \frac{1-t^2}{Q}[\eta_{331}(1-t^2)^2 + \beta^2\eta_{332}(1-t^2)^2 t^2 + \beta^4\eta_{333}t^4]dt$$

$$\bar{G}_{1144} = -2\pi\int_0^1 \frac{1-t^2}{Q}[\eta_{441}(1-t^2)^2 + \beta^2\eta_{442}(1-t^2)^2 t^2 + \beta^4\eta_{443}t^4]dt$$

$$\bar{G}_{1134} = -2\pi \int_0^1 \frac{1-t^2}{Q}[\eta_{341}(1-t^2)^2 + \beta^2\eta_{342}(1-t^2)^2t^2 + \beta^4\eta_{343}t^4]dt$$

$$\bar{G}_{3311} = 2\pi\beta^2 \int_0^1 \frac{t^2}{D}[(\eta_{111}+\eta_{112})(1-t^2)^3 + \beta^2(\eta_{113}+\eta_{114})(1-t^2)^2t^2 + \beta^4(3\eta_{115}+\eta_{116})(1-t^2)t^4 + 2\beta^6\eta_{117}t^6]dt$$

$$\bar{G}_{3333} = -4\pi\beta^2 \int_0^1 \frac{t^2}{Q}[\eta_{331}(1-t^2)^2 + \beta^2\eta_{332}(1-t^2)^2t^2 + \beta^4\eta_{333}t^4]dt$$

$$\bar{G}_{3344} = -4\pi\beta^2 \int_0^1 \frac{t^2}{Q}[\eta_{441}(1-t^2)^2 + \beta^2\eta_{442}(1-t^2)^2t^2 + \beta^4\eta_{443}t^4]dt$$

$$\bar{G}_{3334} = -4\pi\beta^2 \int_0^1 \frac{t^2}{Q}[\eta_{341}(1-t^2)^2 + \beta^2\eta_{342}(1-t^2)^2t^2 + \beta^4\eta_{343}t^4]dt$$

$$\bar{G}_{1212} = \frac{\pi}{2} \int_0^1 \frac{(1-t^2)^2}{D}[\eta_{121}(1-t^2)^2 + \beta^2\eta_{122}(1-t^2)^2t^2 + \beta^4\eta_{123}t^4]dt$$

$$\bar{G}_{1313} = -2\pi\beta^2 \int_0^1 \frac{t^2(1-t^2)}{Q}[\eta_{131}(1-t^2) + \beta^2\eta_{132}t^2]dt$$

$$\bar{G}_{1314} = -2\pi\beta^2 \int_0^1 \frac{t^2(1-t^2)}{Q}[\eta_{141}(1-t^2) + \beta^2\eta_{142}t^2]dt$$

$$\bar{G}_{2222} = \bar{G}_{1111},\ \bar{G}_{2211} = \bar{G}_{1122},\ \bar{G}_{2233} = \bar{G}_{1133},\ \bar{G}_{2244} = \bar{G}_{1144}$$

$$\bar{G}_{2234} = \bar{G}_{1134},\ \bar{G}_{3322} = \bar{G}_{3311},\ \bar{G}_{2323} = \bar{G}_{1313},\ \bar{G}_{2324} = \bar{G}_{1314} \tag{3.48}$$

In the above expressions other terms are as follows,

$$D = -PQ$$

$$P = (C_{11} - C_{12})(1-t^2) + 2C_{44}\beta^2t^2$$

$$Q = q_1(1-t^2)^3 + \beta^2q_2(1-t^2)^2t^2 + \beta^4q_3(1-t^2)t^4 + \beta^6q_4t^6 \tag{3.49}$$

In Eqn. (3.48), η_{ijk} depends on the material properties, i.e., electroelastic constants of the constituents and are listed in detail in Appendix B.

Putting value of the electroelastic Green's function, $\bar{G}_{MJin}$ in Eqn. (3.27), piezoelectric Eshelby tensor, S_{MnAb} for a spheroidal inclusion aligned along the x_3-axis, can now be obtained as follows:

$$S_{1111} = S_{2222} = \frac{1}{4\pi}[C_{11}\bar{G}_{1111} + C_{12}\bar{G}_{1212} + C_{13}\bar{G}_{1313} + e_{31}\bar{G}_{1314}]$$

$$S_{1122} = S_{2211} = \frac{1}{4\pi}[C_{12}\bar{G}_{1111} + C_{11}\bar{G}_{1212} + C_{13}\bar{G}_{1313} + e_{31}\bar{G}_{1314}]$$

$$S_{1133} = S_{2233} = \frac{1}{4\pi}[C_{13}(\bar{G}_{1111} + \bar{G}_{1212}) + C_{33}\bar{G}_{1313} + e_{33}\bar{G}_{1314}]$$

$$S_{1143} = S_{2243} = \frac{1}{4\pi}[e_{31}(\bar{G}_{1111} + \bar{G}_{1212}) + e_{33}\bar{G}_{1313} - \kappa_{33}\bar{G}_{1314}]$$

$$S_{1212} = S_{1221} = S_{2112} = S_{2121} = \frac{1}{8\pi}(C_{11} - C_{12})[\bar{G}_{1122} + \bar{G}_{1212}]$$

$$S_{1313} = S_{1331} = S_{3113} = S_{3131} = S_{2323} = S_{2332} = S_{3223} = S_{3232}$$

$$= \frac{1}{8\pi}[C_{44}(\bar{G}_{1133} + \bar{G}_{3311} + 2\bar{G}_{1313})$$

$$+ e_{15}(\bar{G}_{1134} + \bar{G}_{1314})]$$

$$S_{1341} = S_{3141} = S_{2342} = S_{3242} =$$

$$= \frac{1}{8\pi}[e_{15}(\bar{G}_{1133} + \bar{G}_{3311} + 2\bar{G}_{1313})$$

$$- \kappa_{11}(\bar{G}_{1134} + \bar{G}_{1314})]$$

$$S_{3311} = S_{3322} = \frac{1}{4\pi}[C_{11}\bar{G}_{1313} + C_{12}\bar{G}_{2323} + C_{13}\bar{G}_{3333} + e_{31}\bar{G}_{3334}]$$

$$S_{3333} = \frac{1}{4\pi}[C_{13}(\bar{G}_{1313} + \bar{G}_{2323}) + C_{33}\bar{G}_{3333} + e_{33}\bar{G}_{3334}]$$

$$S_{3343} = \frac{1}{4\pi}[e_{31}(\bar{G}_{1313} + \bar{G}_{2323}) + e_{33}\bar{G}_{3333} - \kappa_{33}\bar{G}_{3334}]$$

$$S_{4113} = S_{4131} = S_{4223} = S_{4232} = \frac{1}{4\pi}[C_{44}(\bar{G}_{1134} + \bar{G}_{1314}) + e_{15}\bar{G}_{1144}]$$

$$S_{4141} = S_{4242} = \frac{1}{4\pi}[e_{15}(\bar{G}_{1134} + \bar{G}_{1314}) - \kappa_{11}\bar{G}_{1144}]$$

$$S_{4311} = S_{4322} = \frac{1}{4\pi}[C_{11}\bar{G}_{1314} + C_{12}\bar{G}_{2324} + C_{13}\bar{G}_{3334} + e_{33}\bar{G}_{3344}]$$

$$S_{4333} = \frac{1}{4\pi}[C_{13}(\bar{G}_{1314} + \bar{G}_{2324}) + C_{33}\bar{G}_{3334} + e_{33}\bar{G}_{3344}]$$

$$S_{4343} = \frac{1}{4\pi}[e_{31}(\bar{G}_{1314} + \bar{G}_{2324}) + e_{33}\bar{G}_{3334} - \kappa_{33}\bar{G}_{3344}]$$

$S_{MnAb} = 0$, otherwise. (3.50)

3.4 Effective Electroelastic Moduli

Now, consider a sufficiently large two-phase piezoelectric composite of domain D consists n number of spatially oriented ellipsoid inhomogeneities denoted by $\Omega\ (= \Omega_1 + \Omega_2 + \cdots + \Omega_n)$ with electroelastic constant L^*_{iJMn}. The surrounding matrix is denoted by $D - \Omega,$ having electroeleastic constant E_{iJMn}. The electroelastic constants are measured in the direction coincident with crystalline directions (x_1, x_2, x_3) of the matrix medium. The Mori-Tanaka mean field theory is employed for predicting effective electroelastic constants of such a piezoelectric composite with randomly oriented inclusions. An inherent advantage of this theory over other theories is of being self-consistent and hence it is being used for the current analysis. The effective properties are being estimated based on two sets of boundary conditions, i.e., a traction-electric displacement prescribed and an elastic displacement-electric field prescribed.

3.4.1 Traction-electric displacement prescribed

Suppose a piezocomposite be subjected to a far-field traction and electric-displacement, $\Sigma^0_{iJ}n_i$, at the boundary with outward unit normal vector n_i. In the absence of any piezoelectric inhomogeneity, the strain and electric field, Z^0_{Mn}, would distribute

uniformly throughout the composite. The presence of any random inhomogeneity Ω_k would cause the disturbance in the local fields of both the matrix as well as kth inhomogeneity in the form of eigen stress and electric displacement. The averages of these distributed disturbances are quantified and represented as, $\langle \Sigma_{iJ}^{m} \rangle$ and $\langle \Sigma_{iJ}^{\Omega} \rangle$. The superscripts m and Ω corresponds to the values measured for the matrix and the kth inhomogeneity, respectively. The angled bracket $\langle \quad \rangle$ around any local field variable denotes the quantities obtained by volume averaging of the field over the entire composite domain, D.

In the absence of any piezoelectric inhomogeneity, the volume average of the disturbance portion of the stress and electric displacement vanishes and is mathematically expressed as

$$\int_D \Sigma_{iJ} d\boldsymbol{x}=0, \tag{3.51}$$

also,

$$(1-f)\langle \Sigma_{iJ}^{m} \rangle + f\langle \Sigma_{iJ}^{\Omega} \rangle = 0, \tag{3.52}$$

where f is the volume fraction of the inhomogeneities, and

$$\Sigma_{iJ}^{m} = \begin{cases} \sigma_{iJ}^{m} & J \leq 3, \\ D_i^{m} & J = 4, \end{cases} \tag{3.53}$$

$$\Sigma_{iJ}^{\Omega} = \begin{cases} \sigma_{iJ}^{\Omega} & J \leq 3, \\ D_i^{\Omega} & J = 4. \end{cases} \tag{3.54}$$

In the presence of any inhomogeneity, the average disturbed stress and electric displacement in the matrix and the kth inhomogeneity, respectively be written as

$$\langle \Sigma_{iJ}^{m} \rangle = L_{iJMn} \langle Z_{Mn}^{m} \rangle \text{ in } D - \Omega \tag{3.55}$$

$$\langle \Sigma_{iJ}^{\Omega_k} \rangle = L_{iJMn}^{*} (\langle Z_{Mn}^{m} \rangle + \langle Z_{Mn} \rangle) \text{ in } \Omega_k. \tag{3.56}$$

In the above equations, $\langle Z_{Mn}^{m} \rangle$ represent the average strain and electric field in the matrix, and $\langle Z_{Mn} \rangle$ represent the average disturbance of the uniform strain and electric field in Ω_k. Since, the geometric shape and the material constants remains same for all inhomogeneities, the average value of any field variable over Ω_k is identical with that of measured over all Ωs, i.e., $\langle \Sigma_{iJ}^{\Omega_k} \rangle = \langle \Sigma_{iJ}^{\Omega} \rangle$.

The average stress and electric displacement in the inhomogeneities, when the piezocomposite is subjected to the boundary condition of uniform far-field mechanical load and electric displacement, Σ_{iJ}^{0}, can be expressed as

$$\Sigma_{iJ}^{0} + \langle \Sigma_{iJ}^{\Omega} \rangle = L_{iJMn}^{*}(Z_{Mn}^{0} + \langle Z_{Mn}^{m} \rangle + Z_{Mn}), \tag{3.57}$$

where Σ_{iJ}^{0} and Z_{Mn}^{0} represent the following field variables:

$$\Sigma_{iJ}^{0} = \begin{cases} \sigma_{ij}^{0} & J \leq 3, \\ D_{i}^{0} & J = 4, \end{cases} \tag{3.58}$$

$$Z_{Mn}^{0} = \begin{cases} \varepsilon_{mn}^{0} & M \leq 3, \\ -E_{i}^{0} & M = 4. \end{cases} \tag{3.59}$$

In Eqn. (3.57), $\langle Z_{Mn} \rangle = Z_{Mn}$ in Ω as, for the ellipsoidal inhomogeneities, the applied electromechanical load is uniform.

The theory of equivalent inclusion method [23] suggests that the stress and electric displacement in any inhomogeneity can be simulated with an equivalent inclusion with the material properties of the surrounding matrix medium and having a fictitious eigenstrain and eigen electric field, Z_{Mn}^{*}. With the help of this theory, Eqn. (3.57) may also be expressed as

$$\Sigma_{iJ}^{0} + \langle \Sigma_{iJ}^{\Omega} \rangle = L_{iJMn}^{*}(Z_{Mn}^{0} + \langle Z_{Mn}^{m} \rangle + Z_{Mn}) = L_{iJMn}(Z_{Mn}^{0} + \langle Z_{Mn}^{m} \rangle + Z_{Mn} - Z_{Mn}^{*}) , \tag{3.60}$$

where, Z_{Mn}, represents the disturbed field and it is related to the fictitious eigen strain and eigen electric field, Z^*_{Mn} by

$$Z_{Mn} = S_{MnAb} Z^*_{Ab} \,, \tag{3.61}$$

S_{MnAb} is the electroelastic Eshelby tensor, same as those derived in Eqn. (3.50).

By substituting Eqn. (3.61) into (3.59), the average disturbance of stress and electric displacement in the inhomogeneity can also be written as

$$\langle \Sigma^{\Omega}_{ij} \rangle = L_{iJMn} \langle Z^m_{Mn} \rangle + L_{iJMn} (S_{MnAb} - I_{MnAb}) Z^*_{Ab} \,, \tag{3.62}$$

where, I_{MnAb} is a set of fourth-order and second-order identity tensors, represented as

$$I_{MnAb} = \begin{cases} (\delta_{ma}\delta_{nb} + \delta_{mb}\delta_{na})/2 & M, A \leq 3 \\ \delta_{nb} & M, A = 4 \\ 0 & Otherwise. \end{cases} \tag{3.63}$$

Eqns. (3.52), (3.56) and (3.62) are combined together and rearranged to get the following expression

$$\langle Z^m_{Mn} \rangle = -f (S_{MnAb} - I_{MnAb}) Z^*_{Ab}. \tag{3.64}$$

Substitution of Eqn. (3.64) into (3.55) and (3.62), respectively, yields the average disturbed stress and electric displacement for the matrix and inhomogeneity, respectively as follows

$$\langle \Sigma^m_{ij} \rangle = -f L_{iJMn} (S_{MnAb} - I_{MnAb}) Z^*_{Ab} \,, \tag{3.65}$$

$$\langle \Sigma^{\Omega}_{ij} \rangle = (1 - f) L_{iJMn} (S_{MnAb} - I_{MnAb}) Z^*_{Ab}. \tag{3.66}$$

By substituting Eqn. (3.64) into the equivalency Eqn. (3.60), the equivalent eigenstrain and eigen electric field, Z^*_{Ab}, are derived as

$$Z^*_{Ab} = -U^{-1}_{AbiJ} \left(L^*_{iJMn} - L_{iJMn} \right) Z^0_{Mn} \,, \tag{3.67}$$

where U^{-1}_{AbiJ} is the inverse of U_{iJAb} and it is written as

$$U_{iJAb} = \left(L^*_{iJMn} - L_{iJMn}\right) \times [(1-f)S_{MnAb} + fI_{MnAb}] + L_{iJAb} \tag{3.68}$$

.

The overall strain and electric field, $\langle Z^c_{Mn} \rangle$, of the piezoelectric composite is obtained by taking a weighted average of these parameters over each phase as

$$\langle Z^c_{Mn} \rangle = \frac{1}{V}\left[\int_{D-\Omega} (Z^0_{Mn} + \langle Z^m_{Mn} \rangle) d\boldsymbol{x} + \int_{\Omega} \left(Z^0_{Mn} + \langle Z^{\Omega}_{Mn} \rangle\right) d\boldsymbol{x}\right], \tag{3.69}$$

where V denotes the overall volume of the composite.

Now, substituting Eqns. (3.61) and (3.64) into (3.69), leads to the equation

$$\langle Z^c_{Mn} \rangle = Z^0_{Mn} + fZ^*_{Mn}. \tag{3.70}$$

With the equivalent eigenstrain and eigen electric field, Z^*_{Mn}, obtained from Eqn. (3.67), the overall strain and electric field $\langle Z^c_{Mn} \rangle$ follows the following expression

$$\langle Z^c_{Mn} \rangle = E^{-1}_{MniJ} \Sigma^0_{iJ}. \tag{3.71}$$

In the above equation, E^{-1}_{MniJ} is the effective electroelastic compliance of the piezoelectric composite and it is given by

$$E^{-1}_{MniJ} = \left[I_{MnAb} - fU^{-1}_{MnqR}\left(L^*_{qRAb} - L_{qRAb}\right)\right] L^{-1}_{AbiJ}\,. \tag{3.72}$$

3.4.2 Elastic displacement-electric field prescribed

When the piezocomposite is subjected to a far-field applied elastic displacement and electric field, Z^0_{Mn}, on the boundary; due to the presence of piezoelectric inhomogeneities, it results into a disturbed strain and electric field in each phase. The volume average of the disturbed strain and electric field distributed over the entire composite must vanish that gives the following expression:

$$(1-f)\langle Z^m_{Mn} \rangle + f\langle Z^{\Omega}_{Mn} \rangle = 0\,, \tag{3.72}$$

where $\langle Z_{Mn}^{m} \rangle$ and $\langle Z_{Mn}^{\Omega} \rangle$ represent the average value of strain and electric field present in the matrix and the inhomogeneities, respectively. Using equivalent inclusion method, the average stress and electric displacement in the inhomogeneities can be obtained as

$$\langle Z_{Mn}^{m} \rangle = -f S_{MnAb} Z_{Ab}^{*} \,, \tag{3.73}$$

$$\langle Z_{Mn}^{\Omega} \rangle = \langle Z_{Mn}^{m} \rangle + Z_{Mn} \,, \tag{3.74}$$

To solve for the equivalent eigen fields, (i.e., eigen strain and eigen electric field), Z_{Mn}^{*}, Eqns. (3.73) and (3.74) are substituted into the equivalency equation (1.60) and yields

$$Z_{Ab}^{*} = -V_{AbiJ}^{-1} \big(L_{iJMn}^{*} - L_{iJMn} \big) Z_{Mn}^{0} \,, \tag{3.75}$$

where V_{AbiJ}^{-1} is the inverse of V_{iJAb}

$$V_{iJAb} = (1-f) \big(L_{iJMn}^{*} - L_{iJMn} \big) S_{MnAb} + L_{iJAb} \,. \tag{3.76}$$

The overall stress and electric displacement, $\langle \Sigma_{iJ}^{c} \rangle$, of the piezoelectric composite holds the same definition as used while deriving Eqn. (3.69) and can be written as

$$\begin{aligned} \langle \Sigma_{iJ}^{c} \rangle &= \frac{1}{V} \left[\int_{D-\Omega} \big(\Sigma_{iJ}^{0} + \langle \Sigma_{iJ}^{m} \rangle \big) d\boldsymbol{x} + \int_{\Omega} \big(\Sigma_{iJ}^{0} + \langle \Sigma_{iJ}^{\Omega} \rangle \big) d\boldsymbol{x} \right] \\ &= L_{iJMn} [Z_{Mn}^{0} + (1-f) \langle Z_{Mn}^{m} \rangle + f (\langle Z_{Mn}^{m} \rangle + Z_{Mn} - Z_{Mn}^{*})] \,. \end{aligned} \tag{3.77}$$

Now, substituting of Eqns. (3.61) and (3.74) into (3.77) leads to:

$$\langle \Sigma_{iJ}^{c} \rangle = L_{iJMn} (Z_{Mn}^{0} - f Z_{Mn}^{*}) \,. \tag{3.78}$$

Further, substitution of Eqn. (3.74) into (3.78) followed by few straightforward manipulations result in:

$$\langle \Sigma_{iJ}^{c} \rangle = E_{iJMn} Z_{Mn}^{0} \,. \tag{3.79}$$

In the above equation, E_{iJMn} is the effective electroelastic moduli and obtained as follows:

$$E_{iJMn} = L_{iJAb}\left[I_{AbMn} + fV_{AbqR}^{-1}\left(L_{qRMn}^{*} - L_{qRMn}\right)\right]. \tag{3.80}$$

The effective electroelastic stiffness, E_{iJMn}, and compliance, E_{MniJ}^{-1}, given by Eqn. (3.80) and Eqn. (3.72), respectively, are reciprocal to each other; or holds the identity of $E_{MniJ}^{-1}E_{iJAb} = I_{MnAb}$. The numerical results calculated on the present model verifies this correlation and hence the self-consistency of the model is validated. With the above derivations, it would be interesting to examine the accuracy of the present model for predicting the effective properties of two-phase piezoelectric composite at the low (dilute) and high concentration limits. An interesting observation is made that as the fiber volume fraction, $f \to 0$, E_{MniJ}^{-1} reduces to the value of L_{MniJ}^{-1}, while as $f \to 1$, E_{MniJ}^{-1} attains the value of L_{MniJ}^{*-1}. In a similar manner, E_{iJMn} tends to approach the value of L_{iJMn} and L_{iJMn}^{*}, as the fiber volume fraction, $f \to 0$ and $f \to 1$, respectively.

3.5 Results and Discussion

The electroelastic Green's function can be represented in two indices notation by utilizing the following mapping of adjacent indices:

$$\begin{aligned} &11\to1,\quad 22\to2,\quad 33\to3,\quad 23\to4,\quad 31\to5,\quad 12\to6,\\ &41\to7,\quad 42\to1,\quad 43\to9. \end{aligned} \tag{3.51}$$

With the help of a MATLAB programme the electroelastic Green's function $\bar{G}_{MJin}$ is plotted in a three dimensional space co-ordinate system by plotting shape variables of ellipsoidal inclusion in the x and y-axis while the value of Green's function in the z-axis. From the expression of Green's function shown in Eqn. (3.49), the surface integral is evaluated using a MATLAB programme and results are plotted. The material constants used in the calculation of the electroelastic Green's function are listed in Table 1. To demonstrate our solutions, we present a numerical result of Green's functions as shown in Figures 3.2-3.11.

Table 3.1 Electroelastic constants of the constituent materials

Material Constants	$BaTiO_3$ (fiber)	PZT-5H (matrix)
C_{11} (GPa)	166	126
C_{12} (GPa)	77	55
C_{13} (GPa)	78	53
C_{33} (GPa)	162	117
C_{44} (GPa)	43	35.3
e_{31} (C/m^2)	-4.4	-6.5
e_{33} (C/m^2)	18.6	23.3
e_{15} (C/m^2)	11.6	17.0
κ_{11} (C^2/Nm^2)	11.2×10^{-9}	15.1×10^{-9}
κ_{33} (C^2/Nm^2)	12.6×10^{-9}	13.0×10^{-9}

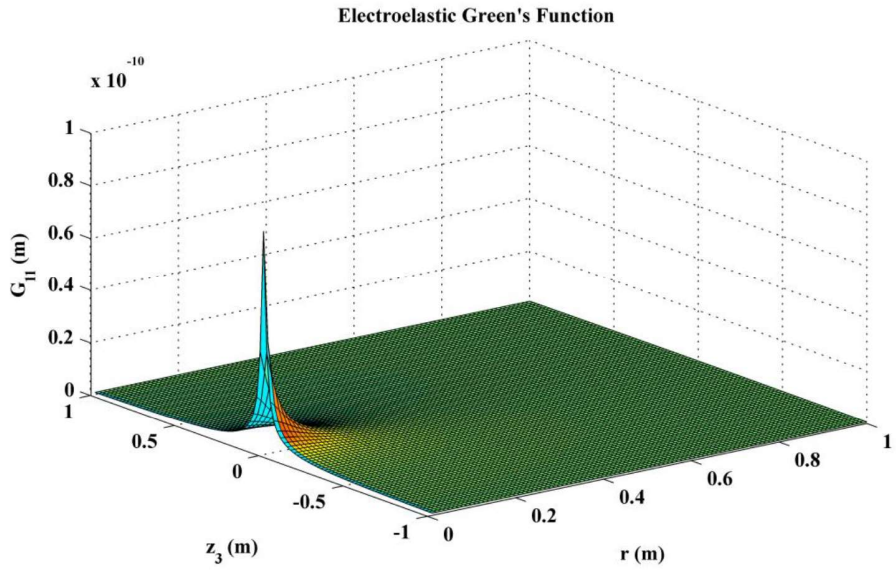

Figure 3.2 The distribution of the Green's function G_{11} in space.

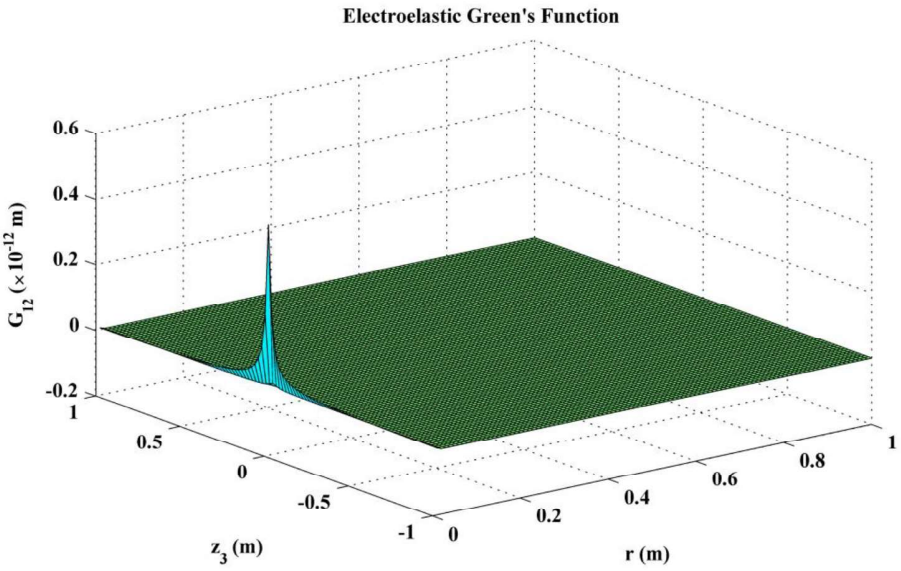

Figure 3.3 The distribution of the Green's function G_{12} in space.

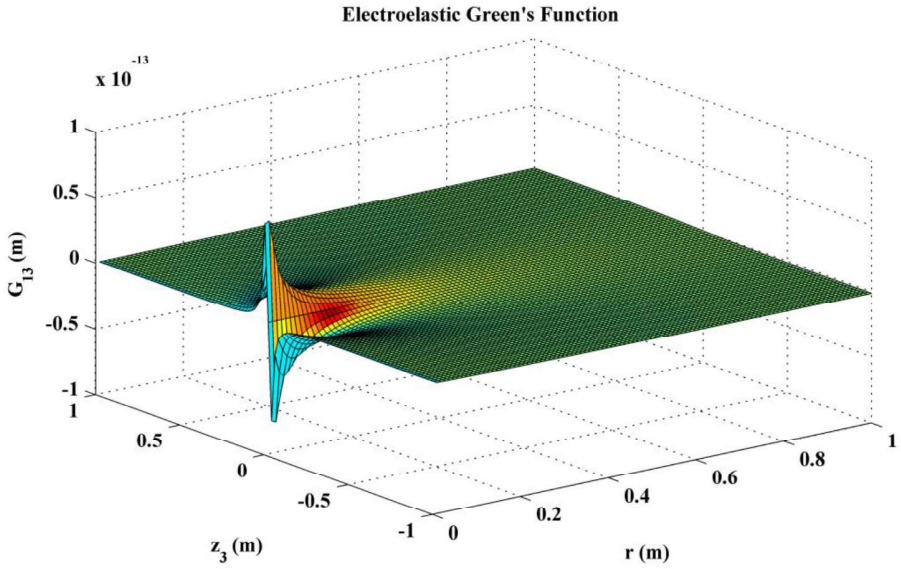

Figure 3.4 The distribution of the Green's function G_{13} in space.

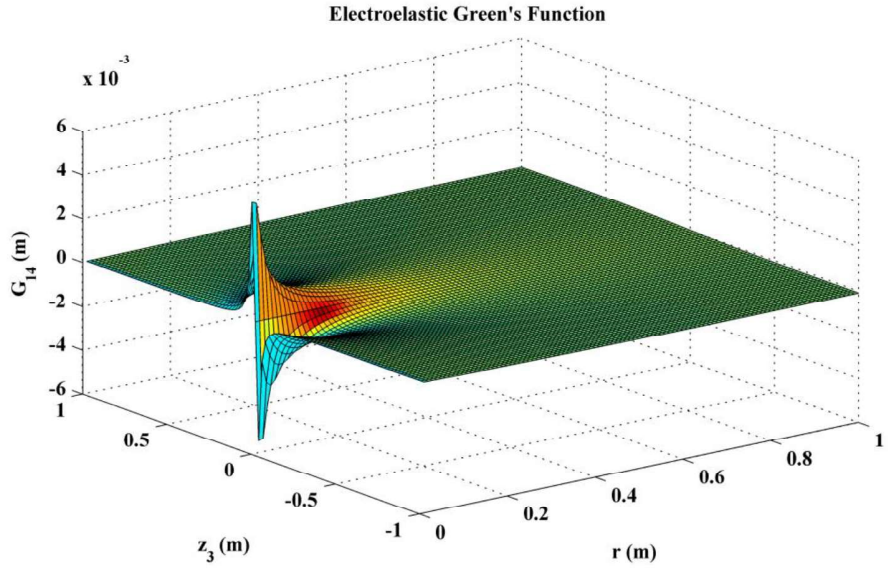

Figure 3.5 The distribution of the Green's function G_{14} in space.

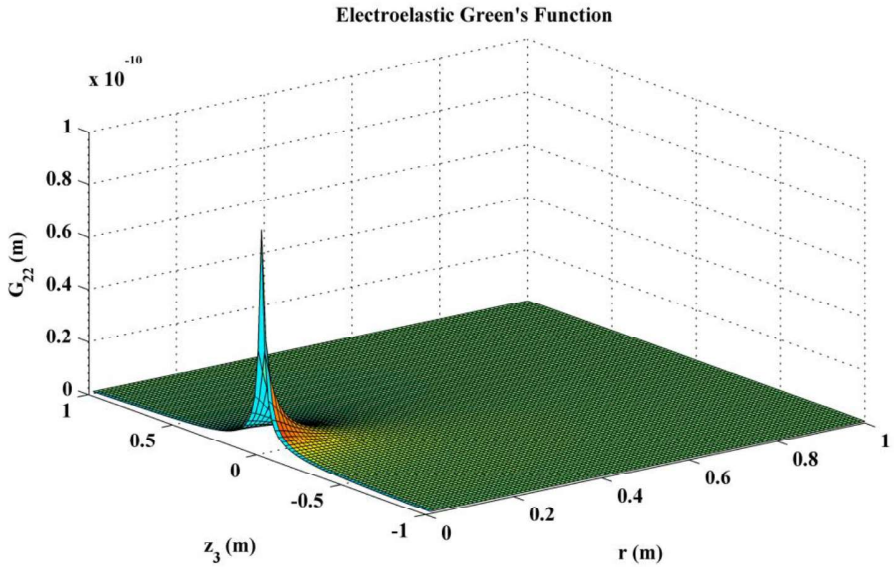

Figure 3.6 The distribution of the Green's function G_{22} in space.

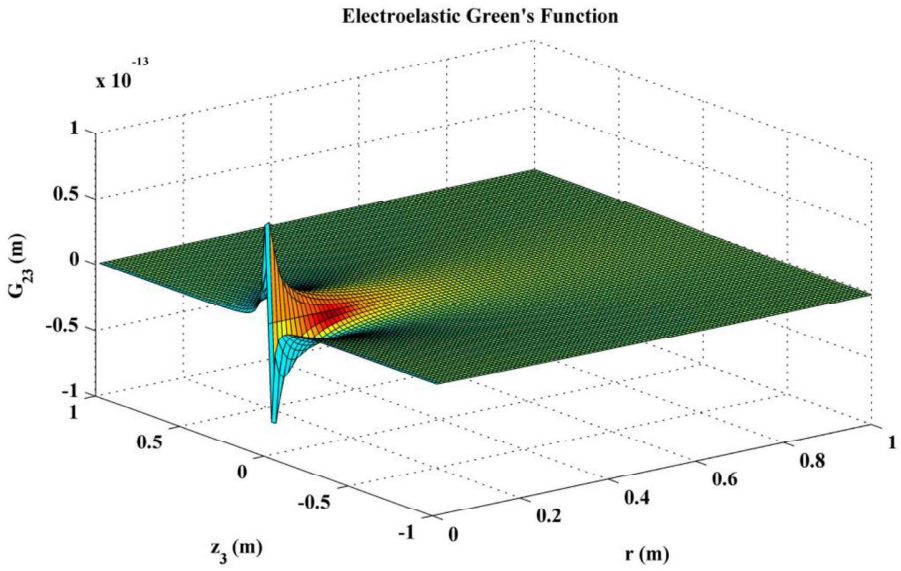

Figure 3.7 The distribution of the Green's function G_{23} in space.

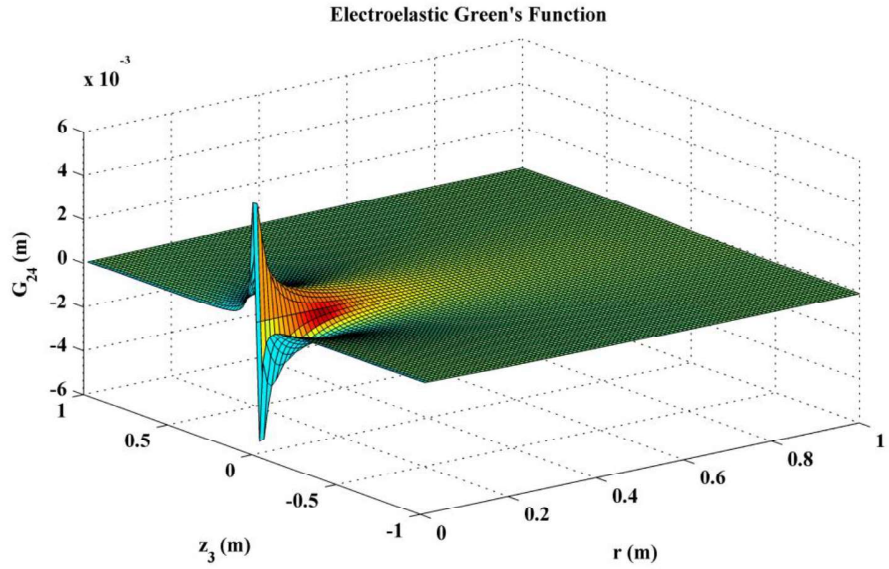

Figure 3.8 The distribution of the Green's function G_{24} in space.

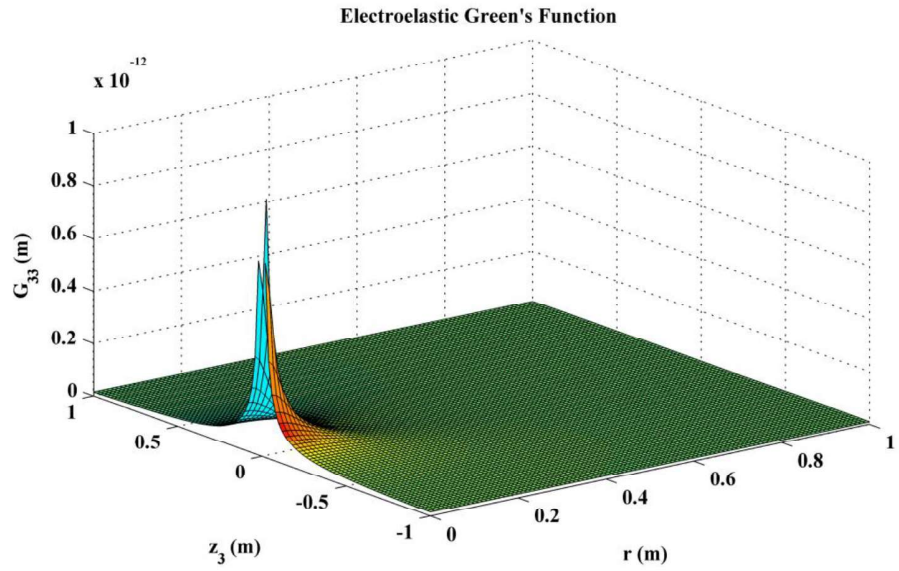

Figure 3.9 The distribution of the Green's function G_{33} in space.

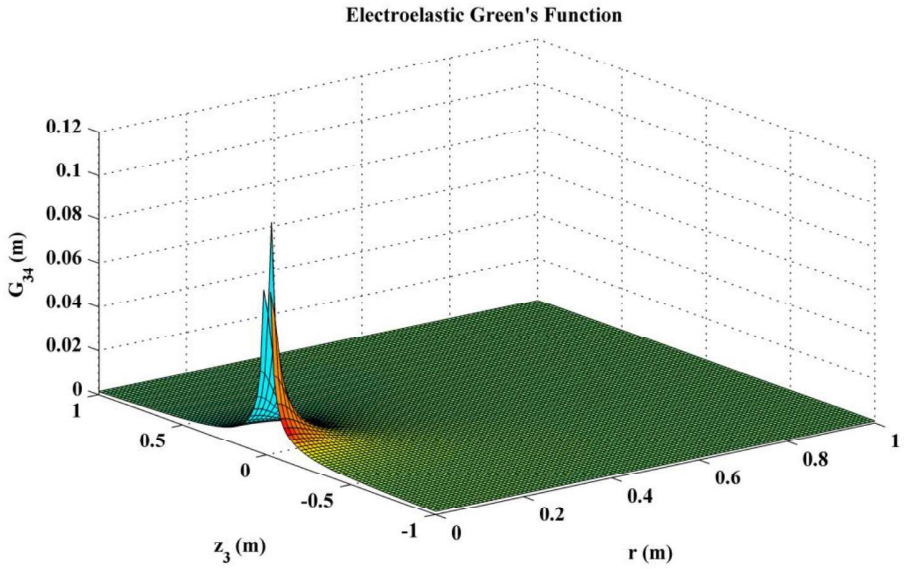

Figure 3.10 The distribution of the Green's function G_{34} in space.

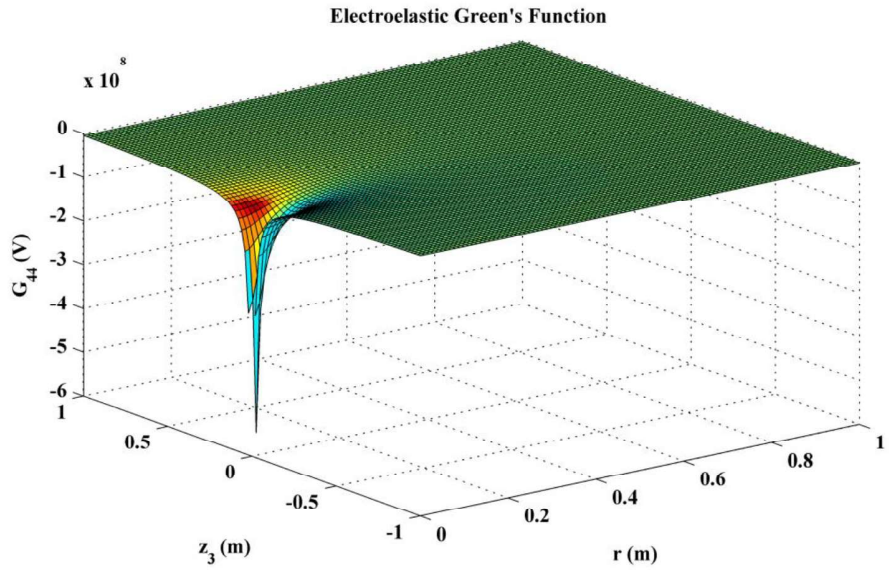

Figure 3.11 The distribution of the Green's function G_{44} in space.

Because all the Green's functions have axial-symmetry along z_3, a surface plot has been generated using two-dimensional cylindrical coordinates r and z_3. Figures 3.2-3.11 demonstrate the distribution of Green's function in whole space and details about Green's functions near the source point. From these figures, it is quite clear that the distributions of different Green's functions are almost similar, while magnitudes vary significantly. The distributions of Green's function G_{11}, G_{12}, G_{22}, G_{33}, G_{34} are showing similar nature but the order of magnitudes of Green's function are slightly different from each other. The other set of Green's functions, i.e., G_{13}, G_{14}, G_{23}, G_{24} shows similarity in distribution in space while G_{13} and G_{23} in pair having same order of magnitudes and G_{14} and G_{24} in another pair having the same order of magnitude.

Eshelby tensors shown in Eqn. (3.50) serve as the cornerstone for the solution of many inclusion problems. The elegance and success of Eshelby tensors for elastic inclusion problems have encouraged authors to explore its utility for simulating

electroelastic response of piezoelectric inclusion. For an ellipsoidal inclusion embedded in a transversely isotropic (6mm symmetry) piezoelectric medium, these tensors can be divided into three categories. The first category consists of those that determines the elastic response under eigenstrains, i.e., S_{1111}, S_{1122}, S_{1133}, S_{3311}, S_{3333}, S_{1313} and S_{1212}. The second category of these tensors are associated with the piezoelectric response due to initial piezoelectric fields of the same kind; these are S_{4141} and S_{4343}. The third category of these tensors are associated with elastic and electric responsive terms S_{1143}, S_{3343}, S_{1341}, S_{4113}, S_{4311}, and S_{4333}. It should be noted that the tensors in the first and second categories are dimensionless, while interactive terms in the third category relating dissimilar physical quantities have dimensions.

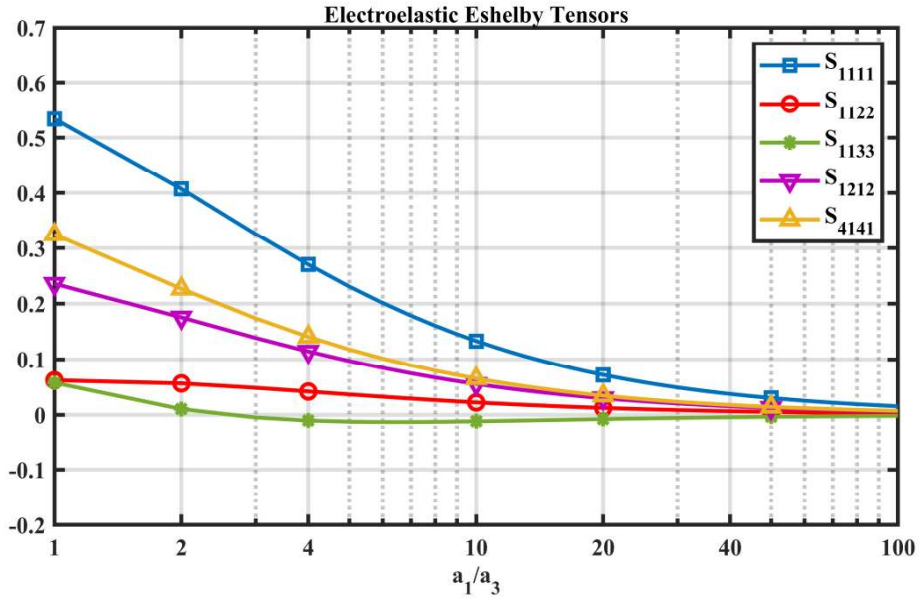

Figure 3.12 Vanishing Eshelby tensors at infinite aspect ratio.

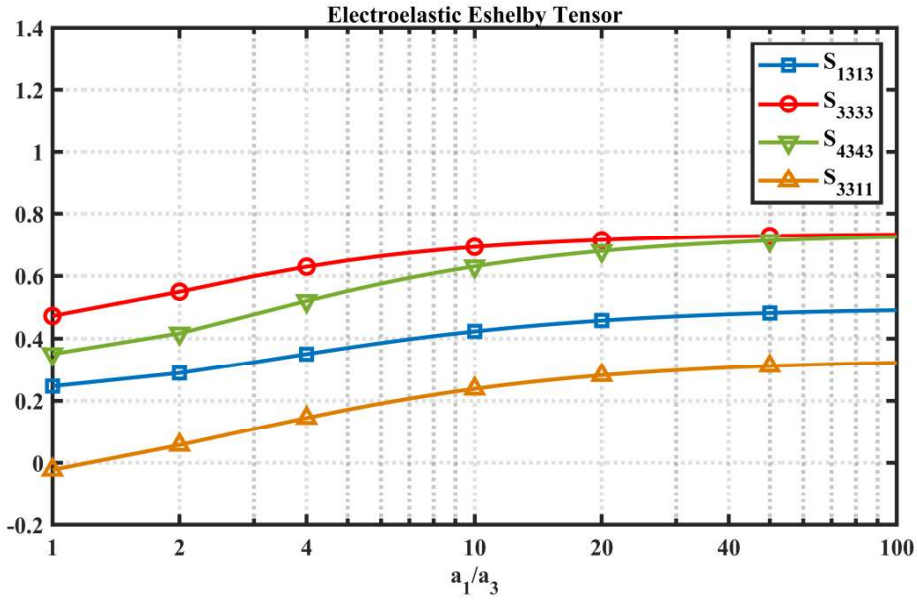

Figure 3.13 Non-vanishing Eshelby tensors at infinite aspect ratio.

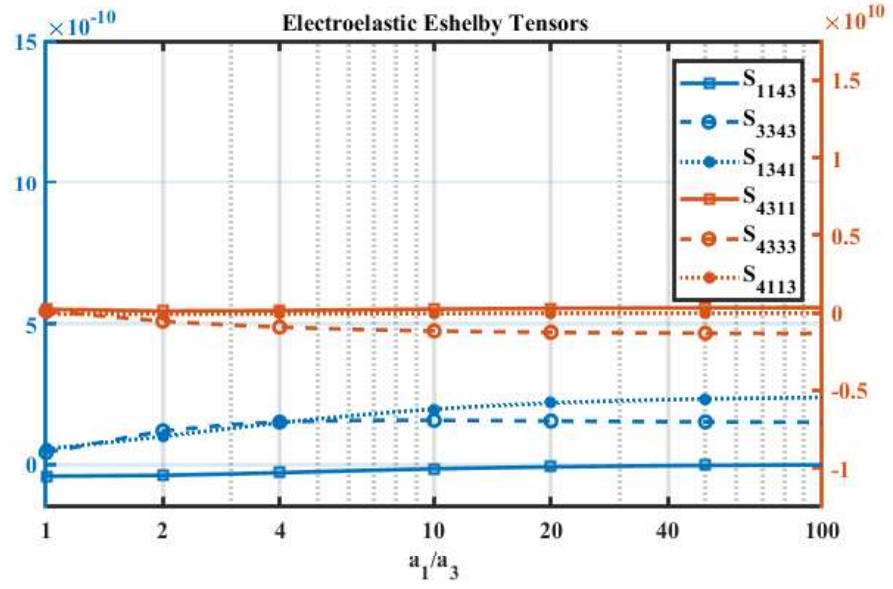

Figure 3.14 Eshelby tensors involving interaction between elastic and electric fields.

Based upon the materials constants given in Table 3.1, the Eshelby tensor elements shown in Eqn. (3.50) has been numerically calculated with the help of MATLAB for

various inclusion aspect ratios, i.e., a_1/a_3 (or α_f). It can be observed from Eqn. (3.50) that there are 15 independent Eshelby tensors. Figure 3.11 shows the group of Eshelby tensors that vanishes at infinite aspect ratio. The tensor elements S_{1111}, S_{1212}, S_{4141} are found to decrease significantly with the ratio while S_{1122}, S_{1133} decreases slightly with the aspect ratio S_{1212} and S_{1143} till it reaches the asymptotic value at $\alpha_f = 10$. Figure 3.13 shows the nonzero elements that vanish at infinite aspect ratio. The tensor elements S_{1313}, S_{3333}, S_{3343} and S_{4343} increases slightly with the aspect ratio till it reaches asymptotic value at $\alpha_f = 10$ as it can be observed from the figure. It is noted that in figure 3.12-3.14, S_{ij4k} and S_{4jik} are of the dimension C/GN and GN/C ($G = 10^9$), respectively, and the other Eshelby tensor elements are nondimensional. It is found that S_{1111}, S_{1122}, S_{1133}, S_{1212}, S_{4141}, S_{4113}, S_{1143} approach zero when the aspect ratio of the inclusion becomes infinite, i.e., continuous fibers. Thus, it can be concluded that for the piezoelectric composites with continuous fibers as inclusions and piezoelectric materials as the matrix, there are only eight nonzero independent Eshelby tensors.

The numerical predictions of the effective electroelastic coefficients for PZT-5H material reinforced by $BaTiO_3$ fibers are calculated using the proposed method. Both the matrix and inhomogeneities are considered to be transversely isotropic (6mm symmetry). The electroelastic material properties of the constituents used in computation have been taken from Table 3.1. The rule-of-mixture that is commonly used in estimating effective elastic properties of composites has a shortcoming that it is modelled on the assumption that strains within a composite are constants. As a result, this rule is a linear combination of constituent's properties weighted by their volume fractions and the geometric shape of the fiber is irrelevant to the results. The method proposed in this section enables the study of influence of the geometric shape of the fiber, i.e., aspect ratio a_f on the overall effective coefficients of the piezoelectric composites.

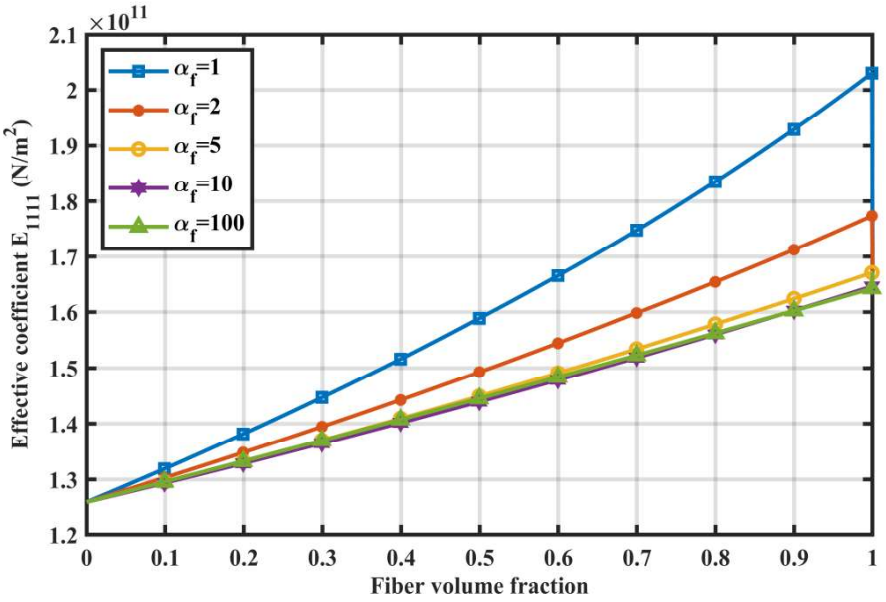

Figure 3.15 The composite normal modulus E_{1111} against fiber volume fraction for various aspect ratios, α_f.

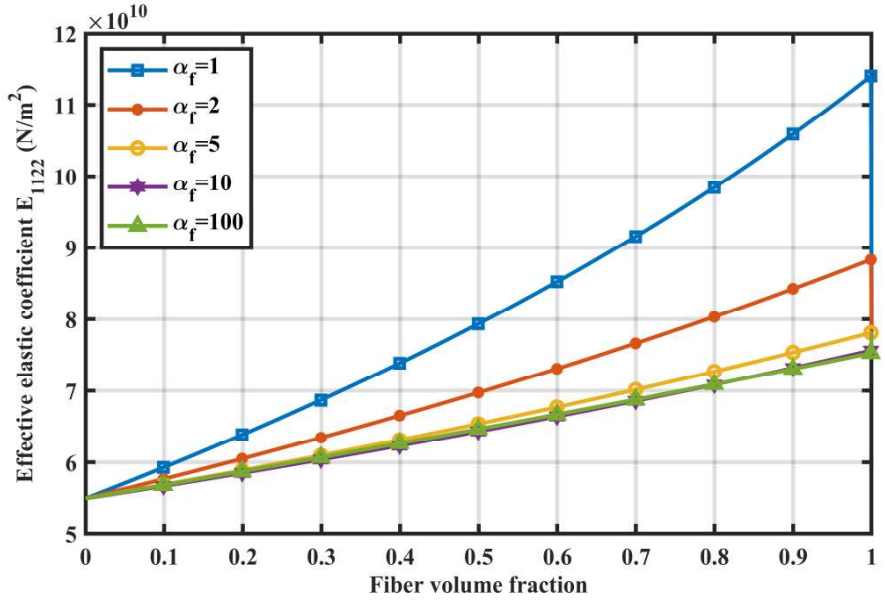

Figure 3.16 The composite normal modulus E_{1122} against fiber volume fraction for various aspect ratios, α_f.

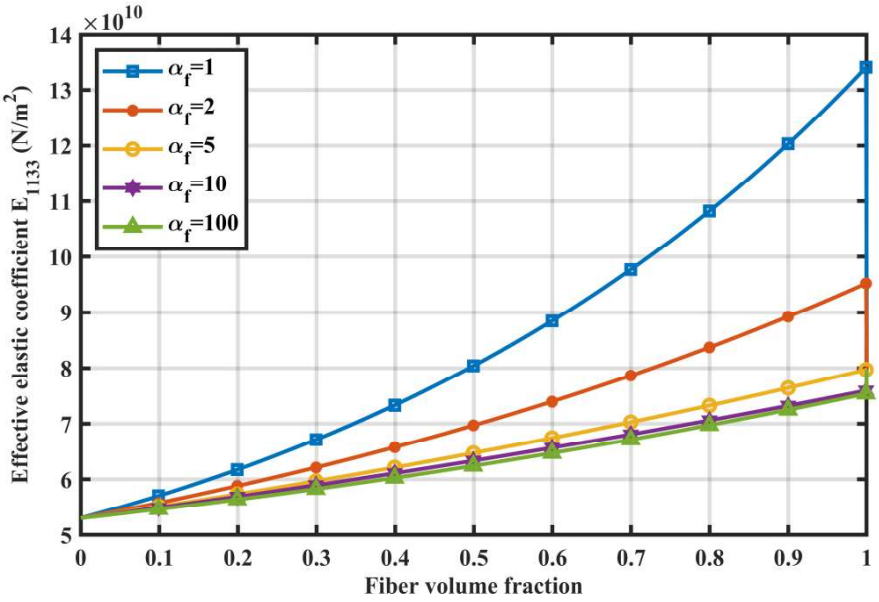

Figure 3.17 The composite normal modulus E_{1133} against fiber volume fraction for various aspect ratios, α_f.

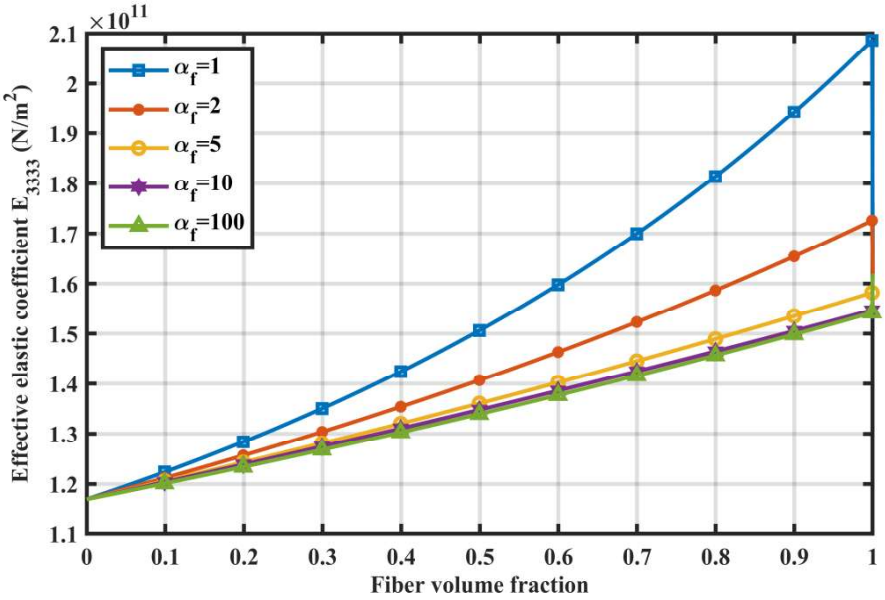

Figure 3.18 The composite normal modulus E_{3333} against fiber volume fraction for various aspect ratios, α_f.

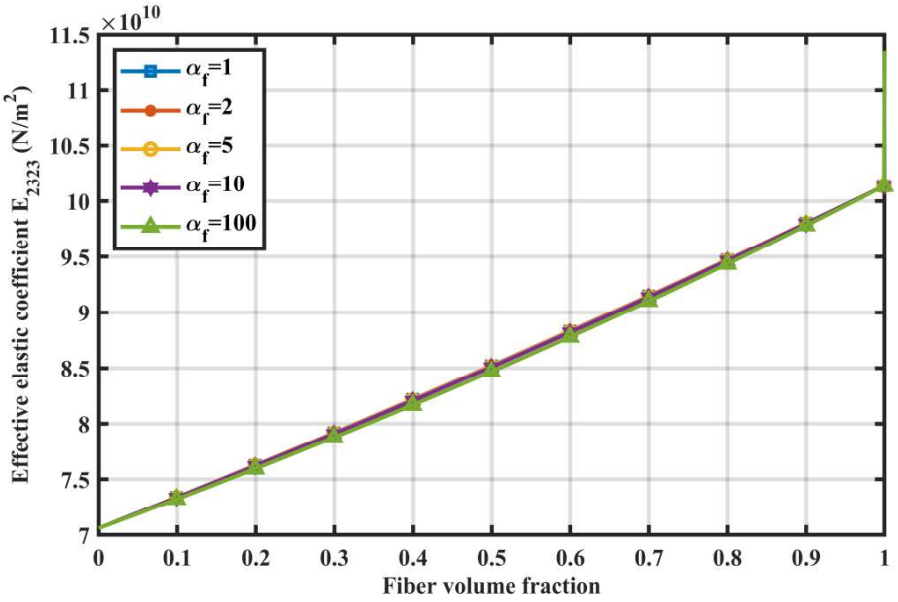

Figure 3.19 The composite shear modulus E_{2323} against fiber volume fraction for various aspect ratios, α_f.

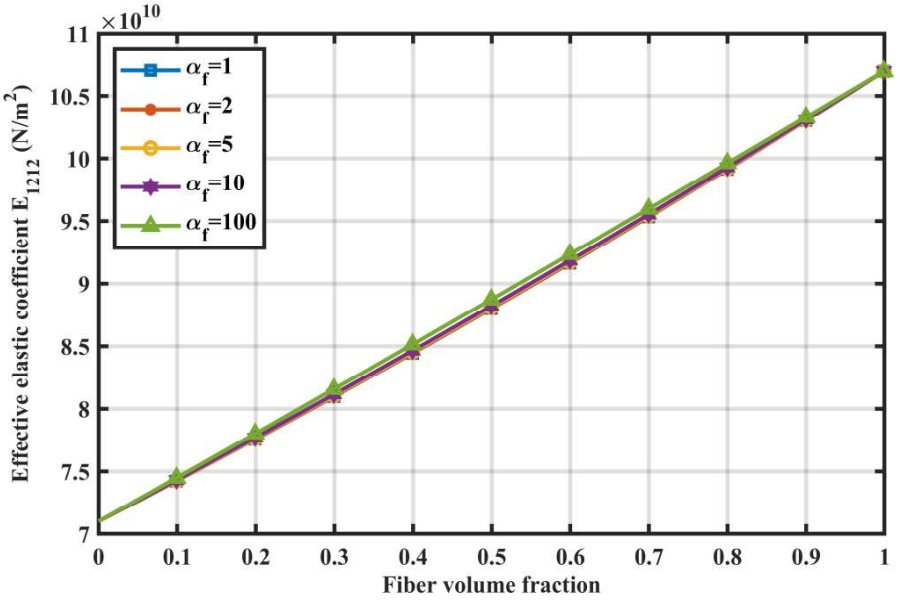

Figure 3.20 The composite shear modulus E_{1212} against fiber volume fraction for various aspect ratios, α_f.

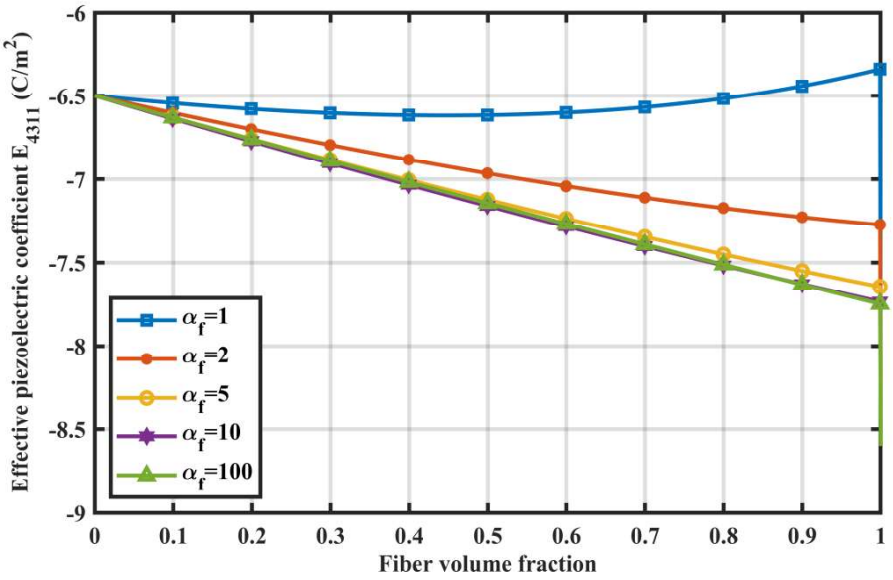

Figure 3.21 The composite piezoelectric constant E_{4311} against fiber volume fraction for various aspect ratios, α_f.

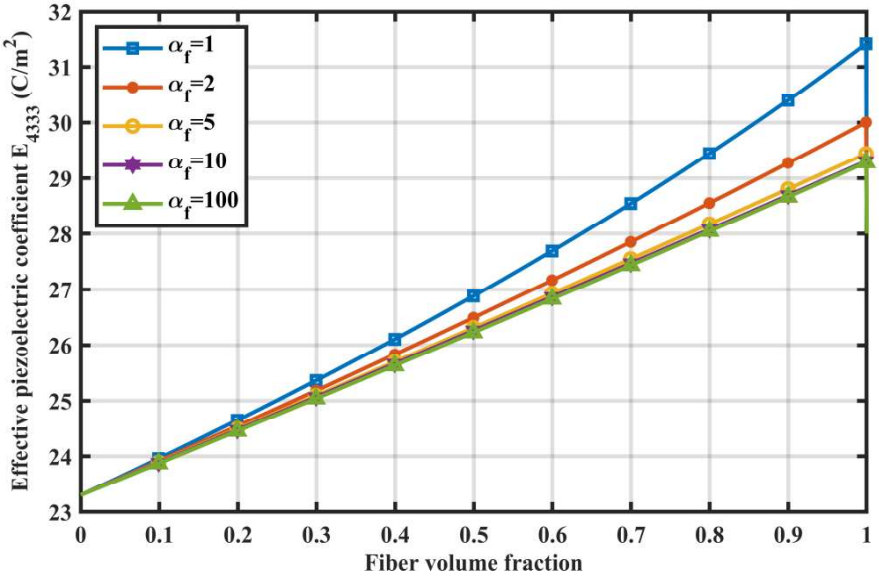

Figure 3.22 The composite piezoelectric constant E_{4333} against fiber volume fraction for various aspect ratios, α_f.

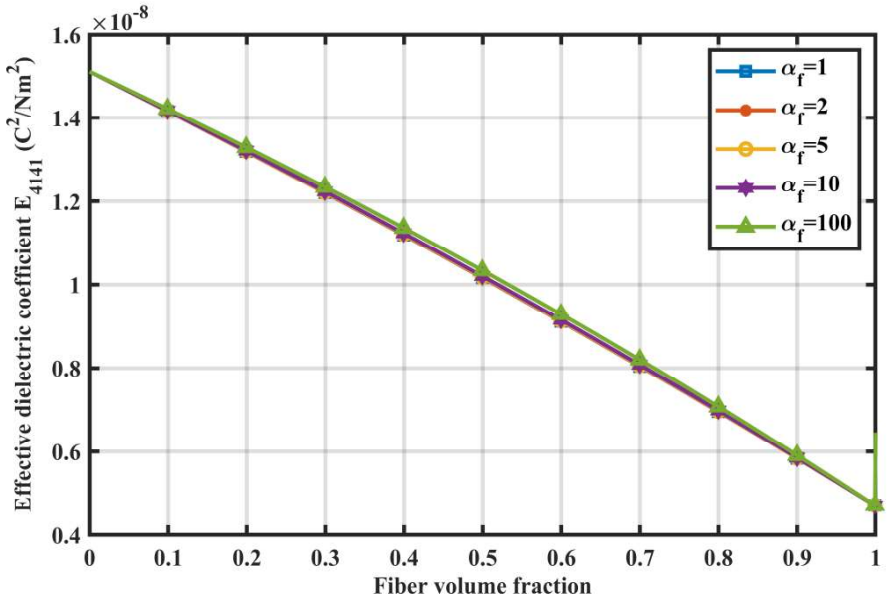

Figure 3.23 The composite dielectric constant E_{4141} against fiber volume fraction for various aspect ratios, α_f.

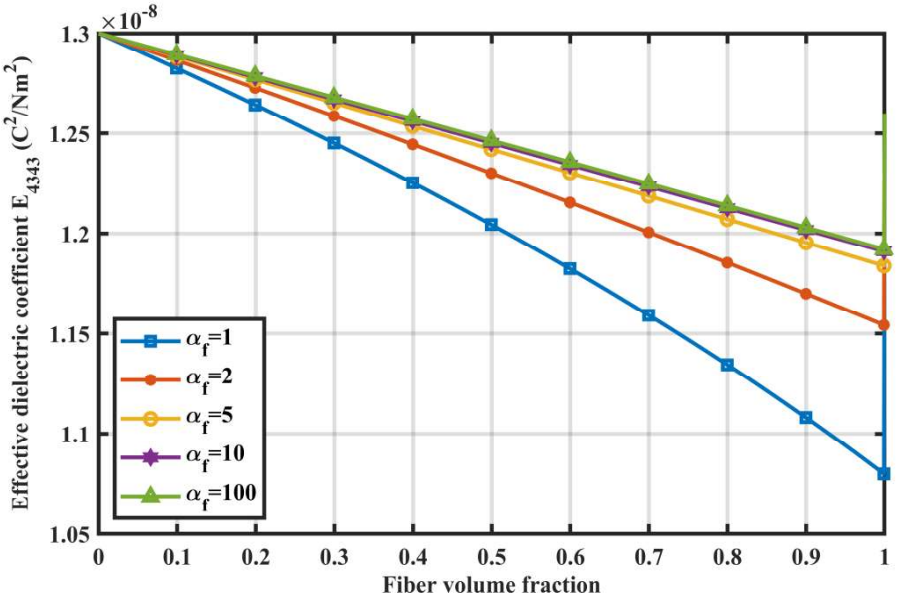

Figure 3.24 The composite dielectric constant E_{4343} against fiber volume fraction for various aspect ratios, α_f.

Figures 3.15-3.18 illustrates the effects of the fiber aspect ratio, a_f on the normal elastic moduli (longitudinal as well as transverse) E_{1111}, E_{1122}, E_{1133} and E_{3333} of the piezoelectric composites. It clearly suggests that similar to the results of the Eshelby tensors at $a_f = 10$; the change in effective elastic moduli with fiber volume fractions attains a limiting value, i.e., the curve traces the same path for the aspect ratios of values greater than 10. Figures 3.19 and 3.20 shows the shear moduli E_{2323} and E_{1212} have less susceptibility to the change in fiber aspect ratio and the curve traces almost same path against the fiber volume fraction for the range of fiber aspect ratio, $\alpha_f = 1$ to 100. Since, there is not much difference in the values for shear elastic moduli of the constituents, i.e., for both fiber as well as matrix phases, the effects of the fiber geometry or inclusion shape are minimal on the overall value of shear moduli of the piezoelectric composite.

The variation of effective piezoelectric constants of composite with change in fiber volume fraction for various aspect ratios a_f is shown in figures 3.21 and 3.22. Both the figure illustrates that the slopes of piezoelectric constants E_{4311} and E_{4333} against fiber volume fraction constantly decreases when plotted for fiber aspect ratio α_f ranging 1 to 100. It should be noted that the value of E_{4311} is negative hence its absolute value increases with increase in fiber aspect ratio. The effects of aspect ratio on dielectric constants of the piezoelectric composite against fiber volume fraction is indicated in figures 3.23 and 3.24. Figure 3.23 clearly suggests that the effects of change in fiber aspect ratio has minimal effect on the dielectric constant E_{4141} when plotted against fiber volume fraction of the piezoelectric composites.

However, it is observed from figure 3.24 that the dielectric constant E_{4343} is highly sensitive to the change in aspect ratio (a_f=1 to 100) though its absolute value is decreasing with increasing fiber aspect ratio. The curves trace similar paths for the aspect ratio a_f of

value equal to or greater than 10 suggests that the reinforcing effects due to fiber length are saturated at this value for all moduli of the piezoelectric composites. In other way, it can be said that $a_f = 10$ is a limiting value, i.e., geometry of fiber with aspect ratio greater than ten doesn't put any substantial effect on the outcome while estimating overall properties of piezoelectric composites.

3.6 Summary

The most significant work to follow the investigation presented in this chapter, is the development of an analytical model for estimating effective electroelastic moduli of a piezoelectric composite. The anisotropic inclusion method has been extended to derive electro-elastic fields due to presence of a piezoelectric inclusion embedded in an infinitely extended piezoelectric matrix. The electro-elastic Eshelby tensors that represent the induction of the strain and electric fields in an inclusion due to the constraint of the surrounding matrix have been obtained. It has been shown that the electro-elastic Eshelby tensors are functions of the shape of inclusion and the properties of the surrounding matrix.

With the explicit expressions for electro-elastic fields in hand, a micromechanics model based on Mori-Tanaka mean-field theory has been derived to predict the effective electro-elastic moduli of the piezoelectric composites. The effect of inclusion-inclusion interaction at finite concentrations has been taken into account while modeling the problem. The effective electro-elastic properties of the composite and the effects of inclusion geometry on the effective properties have been estimated numerically for the $BaTiO_3$/PZT-5H composite (both fiber and matrix phases are piezoelectrically active).